Table 1. Metabolic Parameters in Control Diet (CD) and Diet-Induced Obese (DIO) Mice.

	CD	DIO
Body weight (g)	34.2 ± 0.8	54.1 ± 1.0**
Glucose (mg/dl)	117 ± 7	190 ± 7**
Insulin (μU/ml)	18.9 ± 3.2	126.0 ± 28.7**
Leptin (ng/ml)	2.2 ± 0.6	42.1 ± 4.5**

Results are presented as the mean ± SEM (n = 14). Significantly different from CD mice in each group: **P < 0.01.

Measurement of BDNF and NT-3 content in the brain

BDNF and NT-3 content in the brain of CD and DIO mice fed CD and HFD, respectively, for 16 weeks was measured in accordance with our previous study (3) using commercially available measurement kits for BDNF (BDNF Emax® ImmunoAssay System: Promega Inc., Madison, WI, USA) and for NT-3 (NT-3 Emax® ImmunoAssay System: Promega Inc. Madison, WI).

Western blot analysis of TrkB and TrkC

Western blotting of full-length TrkB and TrkC in the brain of CD and HFD mice was performed in accordance with our previous study (3). Full-length TrkB and TrkC were detected using rabbit polyclonal anti-TrkB antibody (sc-8316; Santa Cruz Biotechnology, Inc., Santa Cruz, CA, USA) and rabbit polyclonal anti-TrkC antibody (sc-14025; Santa Cruz Biotechnology, Inc.), respectively. Results represent the densitometry data relative to glyceraldehyde 3-phosphate dehydrogenase detected in each sample.

Statistical analysis

All values are provided as the mean ± SEM. Statistical analysis of the data was carried out by ANOVA followed by Dunnett's multiple-range test. $P < 0.05$ was considered statistically significant.

Results

Metabolic parameters in CD and DIO mice

The metabolic parameters in CD and DIO mice are shown in Table 1. The body weight of DIO mice was 1.6 times greater than that in CD mice. Plasma levels of glucose, insulin and leptin in DIO mice were significantly high compared to those in CD mice.

Fear-conditioning response

CD mice exhibited 93% freezing as a result of fear in the first session in the contextual conditioning response, and the freezing percentage gradually decreased during the sessions to reach 60% in the fifth session (Fig. 1). In DIO mice, the freezing percentage of the contextual fear response was significantly lower than that in CD mice in each session (Fig. 1). DIO mice exhibited 64% freezing percentage in the first session of the contextual fear response, and the freezing percentage subsequently decreased during the sessions to 23% in the fifth session (Fig. 1). Similarly, the freezing percentage of the cued fear response in DIO mice was 47% in the first session, which was much lower than the 81% in CD mice, and a significant decrease in freezing percentage of DIO mice was observed over the course of three cued sessions compared to CD mice (Fig. 1).

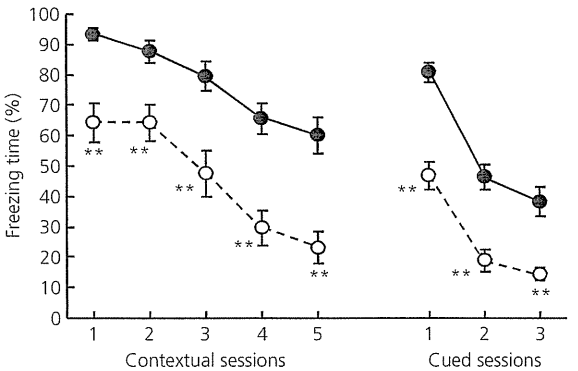

Fig. 1. Fear-conditioning responses in control diet (CD) and diet-induced obese (DIO) mice. Fear-conditioning responses in CD (closed circles) and DIO (open circles) mice. Freezing percentages of CD and DIO mice in the contextual conditioning test were measured every minute for 5 min. Freezing percentages of CD and DIO mice in the cued conditioning test were measured every minute for 3 min. Data points represent the mean ± SEM (n = 9–14). Significantly different from CD mice: *P < 0.05, **P < 0.01.

Jumping–vocalisation test, spontaneous locomotor activity and elevated plus maze test

To compare the sensitivities to foot shock between CD and DIO mice, the jumping–vocalisation test was used. No difference in scores of jumping–vocalisation test was found between CD (score: 3.2 ± 0.3; n = 14) and DIO (score: 2.6 ± 0.1; n = 14) mice. To explore the involvement of motor activity and anxiety in impaired fear-conditioning responses in DIO mice, spontaneous locomotor activity for 30 min after placement of mice into new cages and behaviours in the elevated plus maze test were examined. Spontaneous locomotor activity was not different between CD and DIO mice after 16 weeks of feeding each diet (data not shown). Moreover, both entry times and time spent in the dark and light arms in the elevated plus maze test were not different between CD and DIO mice (data not shown).

BDNF and NT-3 content in the brain areas

BDNF content in the cerebral cortex and hippocampus of DIO mice had significantly decreased to approximately 70% and 60% of CD mice, respectively (Fig. 2A). BDNF content in the amygdala and hypothalamus of DIO mice also tended to decrease compared to that in CD mice (Fig. 2A). By contrast to the changes in BDNF content, NT-3 content in the hippocampus, amygdala and hypothalamus of DIO mice significantly increased to 150%, 165% and 230% of that in CD mice, respectively (Fig. 2B). NT-3 content in the cerebral cortex also tended to be higher than that in CD mice (Fig. 2B).

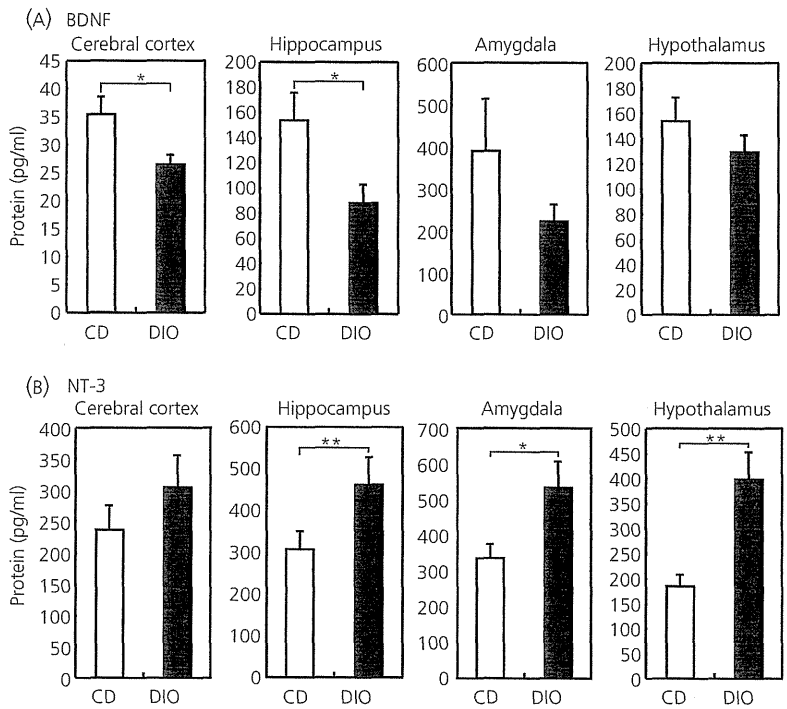

Fig. 2. Content of (A) brain-derived neurotrophic factor (BDNF) and (B) neurotrophin-3 (NT-3) in the cerebral cortex, hippocampus, amygdala and hypothalamus in control diet (CD) and diet-induced obese (DIO) mice. Results are presented as the mean ± SEM (n = 18–29). Significantly different from CD mice: *P < 0.05, **P < 0.01.

Expression of full-length TrkB and TrkC receptors in the brain areas

The expression of full-length TrkB in the amygdala of DIO mice significantly decreased to approximately 70% of CD mice, although not in the cerebral cortex, hippocampus and hypothalamus (Fig. 3A). Full-length TrkC expression in the four brain areas was not significantly different between CD and DIO mice (Fig. 3B).

Discussion

The present study demonstrated that DIO mice showed a significant reduction of both hippocampus-dependent contextual and amygdala-dependent cued fear responses of fear-conditioning test. However, the responses to electric foot shock, locomotor activity and anxiety-like behaviour of DIO mice were the same as those of CD mice. Interestingly, BDNF content in the cerebral cortex and hippocampus of DIO mice was significantly lower than that in CD mice, whereas NT-3 content in the hippocampus, amygdala and hypothalamus of DIO mice was significantly higher than that in CD mice. The expression of full-length TrkB for BDNF in the amygdala of DIO mice significantly decreased compared to that in CD mice, whereas the expression of full-length TrkC for NT-3 in the brain regions was not different between CD and DIO mice. These findings demonstrate that DIO mice display impaired cognition in the fear-conditioning test with an imbalanced interaction between BDNF and NT-3 systems in the cerebral cortex, hippocampus and amygdala related to cognition and fear.

Chronic dietary fat intake, especially saturated fatty acid intake, is reported to contribute to deficits of hippocampus-dependent spatial cognition in the water maze test of rats (5,6,28). The adverse effects of high-dense diets on learning and memory have been associated with impaired hippocampal synaptic plasticity and suppressed neurogenesis (29–31).

Long-term structural alterations of synapses, so-called neuronal plasticity, are regulated by several synaptic molecules including neurotrophic factors, such as BDNF (15), and have been demonstrated to be essential for spatial learning performance, which is dependent primarily on hippocampal functions (15). Animals lacking BDNF show deficits in LTP related to processes of learning and memory, and in hippocampus-dependent spatial learning, which can be amended by exogenous BDNF (15). Although the mechanisms by which a HFD can affect BDNF expression are largely unknown, in the present study, the feeding of HFD or obesity led to a reduction of BDNF content in the hippocampus and cerebral cortex to the extent that cognitive performance was compromised. By contrast to the decrease in BDNF content, the present study demonstrated that NT-3 content was significantly increased in the hippocampus, amygdala and hypothalamus of DIO mice compared to that in CD mice. BDNF and NT-3 oppose one another in regulating

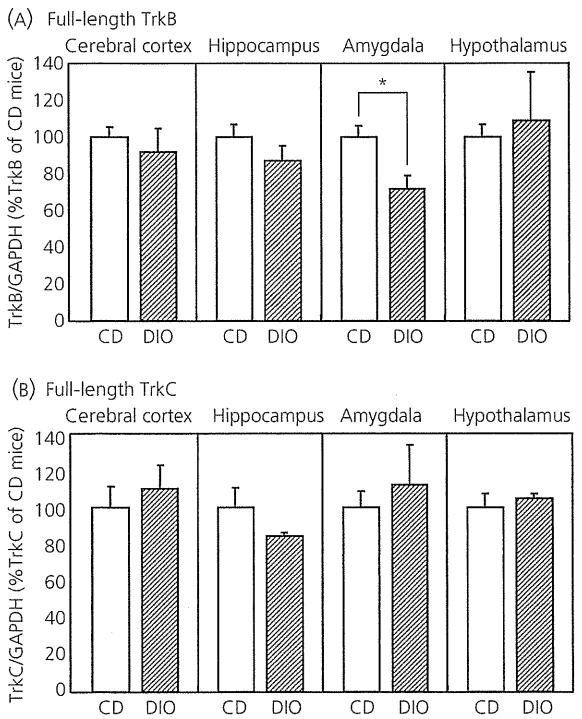

Fig. 3. Expression of full-length TrkB (A) and TrkC (B) in the cerebral cortex, hippocampus, amygdala and hypothalamus in control diet (CD) and diet-induced obese (DIO) mice. Results are presented as the mean ± SEM ($n = 3$–7). Significantly different from CD mice: *$P < 0.05$. GAPDH, glyceraldehyde 3-phosphate dehydrogenase.

the dendritic growth of pyramidal neurones in the hippocampus and neural activity (22,23). NT-3 was reported to inhibit the dendritic growth stimulated by BDNF (22). The amygdala, which is well established as playing a pivotal role in regulation of fear, emotion and cognition (8,9), is suggested to be involved in energy regulation because lesion of the amygdala has been reported to induce hyperphasia, resulting in marked obesity (10,11). Moreover, the amygdala has recently been demonstrated to be one of the brain regions regulating appetite via activation of the melanocortin system (12). Taken together, these findings suggest that the impaired fear-conditioning response in DIO mice is attributed to the decrease of BDNF, which facilitates memory processes and the antagonistic actions of NT-3 against BDNF in the hippocampus and amygdala, although the present study did not address the mechanisms responsible for changes in BDNF and NT-3 content in the brain of DIO mice.

Several lines of electrophysiological and behavioural evidence demonstrate that leptin and insulin enhance hippocampal synaptic plasticity and improve learning and memory (31,32). Electrophysiological studies in genetically obese Zucker rats with leptin-receptor deficiency demonstrated that LTP of the hippocampal CA1 region, which is closely related to learning and the formation of memory and is regulated by NMDA and AMPA receptors (6), is markedly impaired compared to lean rats (7). Streptozotocin-treated insulin-deficient rats are reported to exhibit impaired cognition in the water maze test, which is dependent on the hippocampus (33). Therefore, it is likely that impairment of actions of leptin or insulin might be attributable to cognitive deficits in obesity and diabetes mellitus (34,35). Although there is no direct evidence for the impairment of cognition in DIO mice, the impaired cognitive behaviours of fear-conditioning tests observed in the present study may be partly mediated by decreased inherent functions of leptin and insulin in the brain, despite high plasma levels of leptin and insulin, giving rise to the so-called leptin resistance or insulin resistance associated with obesity.

The present study has shown that DIO mice exhibit impairment of both hippocampus-dependent contextual and amygdala-dependent cued responses of the fear-conditioning test. Moreover, BDNF content decreases in the hippocampus and cerebral cortex of DIO mice, whereas NT-3 content increases in the hippocampus, amygdala and hypothalamus of DIO mice, compared to CD mice. The expression of TrkB in the amygdala of DIO mice decreases compared to CD mice. These findings suggest that consumption of a HFD may contribute to aspects of dysfunction in the central nervous system.

Acknowledgements

This work was supported in part by research grants from the Ministry of Education, Culture, Sports, Science and Technology of Japan and the Ministry of Health, Labour and Welfare of Japan. The authors declare that they have no conflicts of interest.

Received 24 November 2011,
revised 27 March 2012,
accepted 4 April 2012

References

1 Elias MF, Elias PK, Sullivan LM, Wolf PA, D'Agostino RB. Lower cognitive function in the presence of obesity and hypertension: the Framingham heart study. *Int J Obes* 2003; **27**: 260–268.
2 Whitmer RA, Gunderson EP, Barrett-Connor E, Quesenberry CP Jr, Yaffe K. Obesity in middle age and future risk of dementia: a 27 year longitudinal population based study. *BMJ* 2005; **330**: 1360–1364.
3 Yamada N, Katsuura G, Ebihara K, Kusakabe T, Hosoda K, Nakao K. Impaired CNS leptin action is implicated in depression associated with obesity. *Endocrinology* 2011; **152**: 2634–2643.
4 Morton GJ, Cummings DE, Baskin DG, Barsh GS, Schwartz MW. Central nervous system control of food intake and body weight. *Nature* 2006; **443**: 289–295.
5 Molteni R, Barnard RJ, Ying Z, Roberts CK, Gómez-Pinilla F. A high-fat, refined sugar diet reduces hippocampal brain-derived neurotrophic factor, neuronal plasticity, and learning. *Neuroscience* 2002; **112**: 803–814.
6 Neves G, Cooke SF, Bliss TV. Synaptic plasticity, memory and the hippocampus: a neural network approach to causality. *Nat Rev Neurosci* 2008; **9**: 65–75.
7 Gerges NZ, Aleisa AM, Alkadhi KA. Impaired long-term potentiation in obese zucker rats: possible involvement of presynaptic mechanism. *Neuroscience* 2003; **120**: 535–539.
8 Weiskrantz L. Behavioral changes associated with ablations of the amygdaloid complex in monkeys. *J Comp Physiol Psychol* 1956; **49**: 381–391.

9 Fuster JM, Uyeda AA. Reactivity of limbic neurons of the monkey to appetitive and aversive signals. *Electroencephalogr Clin Neurophysiol* 1971; **30**: 281–293.

10 Rollins B, King BM. Amygdala-lesion obesity: what is the role of the various amygdaloid nuclei? *Am J Physiol Regul Integr Comp Physiol* 2000; **279**: R1348–R1356.

11 King BM. Amygdaloid lesion-induced obesity: relation to sexual behavior, olfaction, and the ventromedial hypothalamus. *Am J Physiol Regul Integr Comp Physiol* 2006; **291**: R1201–R1214.

12 Boghossian S, Park M, York DA. Melanocortin activity in the amygdala controls appetite for dietary fat. *Am J Physiol Regul Integr Comp Physiol* 2010; **298**: R385–R393.

13 Burns ME, Augustine GJ. Synaptic structure and function: dynamic organization yields architectural precision. *Cell* 1995; **83**: 187–194.

14 Poo MM. Neurotrophins as a synaptic modulator. *Nat Rev Neurosci* 2001; **2**: 24–32.

15 Korte M, Carroll P, Wolf E, Brem G, Thoenen H, Bonhoeffer T. Hippocampal long-term potentiation is impaired in mice lacking brain-derived neurotrophic factor. *Proc Natl Acad Sci USA* 1995; **92**: 8856–8860.

16 Barbacid M. The Trk family of neurotrophin receptors. *J Neurobiol* 1994; **25**: 1386–1403.

17 Patapoutrian A, Reichardt LF. Trk receptors: mediators of neurotrophin action. *Curr Opin Neurobiol* 2001; **11**: 272–280.

18 Tonra JR, Ono M, Liu X, Garcia K, Jackson C, Yancopoulos GD, Wiegand SJ, Wong V. Brain-derived neurotrophic factor improves blood glucose control and alleviates fasting hyperglycemia in C57BLKS-Lepr(db)/lepr(db) mice. *Diabetes* 1999; **48**: 588–594.

19 Nakagawa T, Ogawa Y, Ebihara K, Yamanaka M, Tsuchida A, Taiji M, Noguchi H, Nakao K. Anti-obesity and anti-diabetic effects of brain-derived neurotrophic factor in rodent models of leptin resistance. *Int J Obes Relat Metab Disord* 2003; **27**: 557–565.

20 Musumeci G, Minichiello L. BDNF-TrkB signalling in fear learning: from genetics to neural networks. *Rev Neurosci* 2011; **22**: 303–315.

21 Malcangio M, Lessmann V. A common thread for pain and memory synapses? Brain-derived neurotrophic factor and trkB receptors. *Trends Pharmacol Sci* 2003; **24**: 116–1121.

22 McAllister AK, Katz LC, Lo DC. Opposing roles for endogenous BDNF and NT-3 in regulating cortical dendrite growth. *Neuron* 1997; **18**: 767–778.

23 Adamson CL, Reid MA, Davis RL. Opposite actions of brain-derived neurotrophic factor and neurotrophin-3 on firing features and ion channel composition of murine spiral ganglion neurons. *J Neurosci* 2002; **22**: 1385–1396.

24 Smith MA, Makino S, Kvetnansky R, Post RM. Stress and glucocorticoids affect the expression of brain-derived neurotrophic factor and neurotrophin-3 mRNAs in the hippocampus. *J Neurosci* 1995; **15**: 1768–1777.

25 Kim JJ, Jung MW. Neural circuits and mechanisms involved in Pavlovian fear conditioning: a critical review. *Neurosci Biobehav Rev* 2006; **30**: 188–202.

26 Weeber EJ, Atkins CM, Selcher JC, Varga AW, Mirnikjoo B, Paylor R, Leitges M, Sweatt JD. A role for the β isoform of protein kinase C in fear conditioning. *J Neurosci* 2000; **20**: 5906–5914.

27 Asakawa A, Inui A, Kaga T, Yuzuriha H, Nagata T, Fujimiya M, Katsuura G, Makino S, Fujino MA, Kasuga M. A role of ghrelin in neuroendocrine and behavioral responses to stress in mice. *Neuroendocrinology* 2001; **74**: 143–147.

28 Kaplan RJ, Greenwood CE. Dietary saturated fatty acids and brain function. *Neurochem Res* 1998; **23**: 615–626.

29 Greenwood CE, Winocur G. Learning and memory impairment in rats fed a high saturated fat diet. *Behav Neural Biol* 1990; **53**: 74–87.

30 Lindqvist A, Mohapel P, Bouter B, Frielingsdorf H, Pizzo D, Brundin P, Erlanson-Albertsson C. High-fat diet impairs hippocampal neurogenesis in male rats. *Eur J Neurol* 2006; **13**: 1385–1388.

31 Farr SA, Yamada KA, Butterfield DA, Abdul HM, Xu L, Miller NE, Banks WA, Morley JE. Obesity and hypertriglyceridemia produce cognitive impairment. *Endocrinology* 2008; **149**: 2628–2636.

32 Wickelgren I. Tracking insulin to the mind. *Science* 1998; **280**: 517–519.

33 Gispen WH, Biessels GJ. Cognition and synaptic plasticity in diabetes mellitus. *Trends Neurosci* 2000; **23**: 542–549.

34 Greenwood CE, Winocur G. High-fat diets, insulin resistance and declining cognitive function. *Neurobiol Aging* 2005; **265**: S42–S45.

35 Myers MG, Cowley MA, Münzberg H. Mechanisms of leptin action and leptin resistance. *Annu Rev Physiol* 2008; **70**: 537–556.

METABOLISM CLINICAL AND EXPERIMENTAL 62 (2013) 70–78

Available online at www.sciencedirect.com

Metabolism

www.metabolismjournal.com

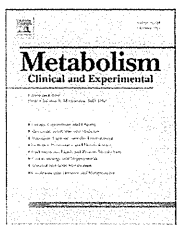

GPR119 expression in normal human tissues and islet cell tumors: evidence for its islet-gastrointestinal distribution, expression in pancreatic beta and alpha cells, and involvement in islet function

Shinji Odori[a], *Kiminori Hosoda*[a,*], *Tsutomu Tomita*[a], *Junji Fujikura*[a], *Toru Kusakabe*[a], *Yoshiya Kawaguchi*[b], *Ryuichiro Doi*[b], *Kyoichi Takaori*[b], *Ken Ebihara*[a], *Yoshiharu Sakai*[b], *Shinji Uemoto*[b], *Kazuwa Nakao*[a]

[a] *Department of Medicine and Clinical Science, Kyoto University Graduate School of Medicine, 54 Shogoin Kawahara-cho, Sakyo-ku, Kyoto 606–8507, Japan*

[b] *Department of Surgery, Kyoto University Graduate School of Medicine, 54 Shogoin Kawahara-cho, Sakyo-ku, Kyoto 606–8507, Japan*

ARTICLE INFO

Article history:
Received 25 April 2012
Accepted 27 June 2012

Keywords:
Insulinoma
Glucagonoma
Insulin secretion
Gastrointestinal hormones

ABSTRACT

Objective. GPR119 is reportedly involved in regulating glucose metabolism and food intake in rodents, but little is known about its expression and functional significance in humans. To begin to assess the potential clinical importance of GPR119, the distribution of GPR119 gene expression in humans was examined.

Materials/Methods. Expression of GPR119 mRNA in fresh samples of normal human pancreas ($n=19$) and pancreatic islets ($n=3$) and in insulinomas ($n=2$) and glucagonomas ($n=2$), all collected at surgery, was compared with the mRNA expression of various receptors highly expressed and operative in human pancreatic islets.

Results. GPR119 mRNA was most abundant in the pancreas, followed by the duodenum, stomach, jejunum, ileum and colon. Pancreatic levels of GPR119 mRNA were similar to those of GPR40 mRNA and were higher than those of GLP1R and SUR1 mRNA, which are strongly expressed in human pancreatic islets. Moreover, levels of GPR119 mRNA in pancreatic islets were more than 10 times higher than in adjacent pancreatic tissue, as were levels of GPR40 mRNA. GPR119 mRNA was also abundant in two cases of insulinoma and two cases of glucagonoma, but was undetectable in a pancreatic acinar cell tumor. Similar results were obtained with mouse pancreatic islets, MIN6 insulinoma cells and alpha-TC glucagonoma cells.

Conclusions. The results provide evidence of an islet-gastrointestinal distribution of GPR119, its expression in pancreatic beta and alpha cells, and its possible involvement in islet function. They also provide the basis for a better understanding of the potential clinical importance of GPR119.

Abbreviations: FFPE, formalin-fixed, paraffin-embedded; GLP1R, glucagon-like peptide 1 receptor; GPR119, G protein-coupled receptor 119; GPR40, G protein-coupled receptor 40; SUR1, sulfonylurea receptor 1.

* *Corresponding author.* Tel.: +81 75 751 3172; fax: +81 75 771 9452.
E-mail address: kh@kuhp.kyoto-u.ac.jp (K. Hosoda).

0026-0495/$ – see front matter © 2013 Elsevier Inc. All rights reserved.
http://dx.doi.org/10.1016/j.metabol.2012.06.010

1. Introduction

Endogenous lipids such as free fatty acids and acylethanolamides are known to regulate glucose metabolism and food intake [1–3]. The underlying molecular mechanisms are not fully understood, however. Recently, four orphan G protein-coupled receptors (GPR40, GPR41, GPR43 and GPR120) were deorphaned and identified as fatty acid receptors [4–8]. Among those, we found that GPR40 is highly expressed in human pancreatic beta cells and is involved in regulating insulin secretion [9,10]. In addition, GPR119 has been identified as a Gs-coupled receptor whose putative endogenous ligands include oleoylethanolamide (OEA) [11,12] and possibly other lipids [13–16]. *In vitro* studies have implicated GPR119 in the regulation of insulin and incretin secretion [12,14,15,17–20], and *in vivo* studies in rats and mice suggest its involvement in the regulation of glucose metabolism and feeding [11,14,18,19,21–30]. That said, glucose metabolism in humans and mice may differ [31], and little is known about the expression and physiological significance of GPR119 in humans.

In that context, we examined GPR119 gene expression in various human tissues, including fresh samples of pancreas and digestive tract collected at surgery. In addition, to gain further insight into the localization of GPR119 within the human pancreas, we compared *GPR119* expression in human pancreatic islets and adjacent pancreatic tissue, as well as in insulinomas and glucagonomas, two very rare human tumors that possess the endocrine properties of pancreatic beta and alpha cells, respectively. The results provide evidence of the islet-gastrointestinal distribution of GPR119, its expression in pancreatic beta and alpha cells, and its possible involvement in islet function in humans.

Table 1 – Clinical profiles of the patients who underwent pancreatectomy and tissues analyzed.

Patient	Age (years)	Sex (M/F)	Disease	Tissue analyzed
1	26	M	Pancreatic cancer	Pancreas (tail)
2	47	F	Pancreatic cancer	Pancreas (head)
3	53	F	Pancreatic cancer	Pancreas (head)
4	54	M	Pancreatic cancer	Pancreas (head)
5	55	F	Pancreatic cancer	Pancreas (body)
6	57	M	Islet cell tumor (nonfunctional)	Pancreas (tail)
7	59	F	Insulinoma	Pancreas (head), insulinoma
8	60	M	Pancreatic cancer	Pancreas (body)
9	60	M	Pancreatic cancer	Pancreas (head)
10	61	F	Papilla cancer	Pancreas (head)
11	63	F	Islet cell tumor (nonfunctional)	Pancreas (body)
12	63	M	Pancreatic cancer	Pancreas (head)
13	64	M	Pancreatic cancer	Pancreas (body)
14	69	M	Pancreatic cancer	Pancreas (head)
15	71	F	Pancreatic cancer	Pancreas (body)
16	72	F	Pancreatic cancer	Pancreas (body)
17	72	F	Pancreatic cancer	Pancreas (head)
18	75	M	Pancreatic cancer	Pancreas (head)
19	76	M	Duodenal cancer	Pancreas (head)
20	27	F	Insulinoma	Insulinoma
21	23	F	Glucagonoma	Glucagonoma
22	41	F	Acinar cell tumor	Acinar cell tumor
23	34	F	Glucagonoma	Glucagonoma

Patients were premedicated with 0.01 mg/kg atropine sulfate i.m. and 0.2 mg/kg diazepam orally before surgery. Tissues were sampled under general anesthesia with 35% O_2, 65% N_2O and 0.5%–1.5% sevoflurane. Neuromuscular blockade was provided by vecuronium bromide at an initial dose 0.1 mg/kg and supplemented as required.

2. Methods

2.1. *Subjects, tissue sampling and pancreatic islet isolation*

The clinical profiles of all patients enrolled in the present study are shown in Table 1. The study was performed in accordance with the Declaration of Helsinki and approved by the Ethical Committee on Human Research of Kyoto University Graduate School of Medicine. Signed informed consent was obtained from all patients.

Normal human cerebral tissues ($n=3$) were collected from three patients at autopsy; one had died from amyotrophic lateral sclerosis, one from an iliopsoas muscle tumor and one from a ruptured aortic aneurysm. Normal tissues from the pancreas ($n=19$), esophagus ($n=3$), stomach ($n=3$), duodenum ($n=3$), jejunum ($n=3$), ileum ($n=2$), colon ($n=3$) and liver ($n=2$) were collected from 23 patients at tumor resection. In Fig. 1B and C, pancreatic tissues from four patients (patients 9, 10, 13 and 19 in Tables 1 and 2) were analyzed because of the limited amount of total RNA extracted from each patient. In all cases, sample margins contained no sign of tumor invasion, so the samples were considered to be tumor-free. In addition, samples of insulinoma ($n=2$), glucagonoma ($n=1$) and a pancreatic acinar cell tumor ($n=1$) were collected at surgery. From another patient with a glucagonoma, samples of normal pancreatic tissue and glucagonoma were obtained as formalin-fixed, paraffin-embedded (FFPE) sections. Islets were promptly isolated from pancreatic samples using the mince method and were collected manually using a stereomicroscope [9,10]. In Japan, HbA1c is measured using high-performance liquid chromatography with a set of calibrators assigned by the Japan Diabetes Society (normal range 4.3%–5.8%). A correlational analysis showed that, in Japan, estimated HbA1c values are 0.4% lower than those measured by the National Glycohemoglobin Standardization Program (NGSP) [32]. For that reason, we standardized the obtained HbA1c values to NGSP units by adding 0.4% to the measured values.

2.2. *Preparation and culture of mouse pancreatic islets, the MIN6 mouse insulinoma cell line and the alpha-TC mouse glucagonoma cell line*

Male 14-week-old C57BL/6 mice were purchased from Japan SLC (Shizuoka, Japan) and housed in a temperature-, humidity- and light-controlled room with free access to water and standard chow (Nosan, Kanagawa, Japan). Mouse pancreatic islets were isolated as previously described [33]. All experimental procedures were approved by the Animal Research

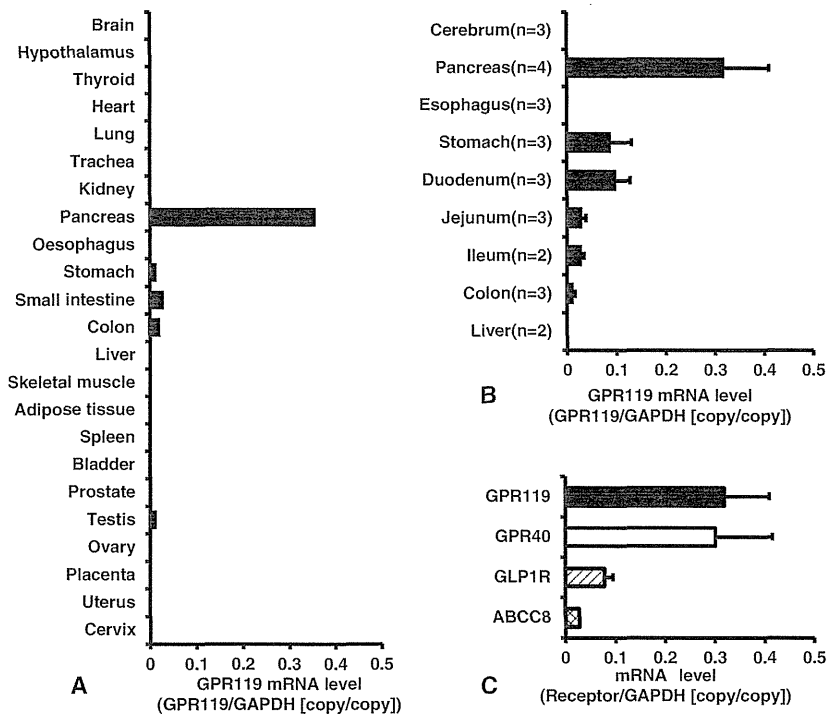

Fig. 1 – Expression of GPR119 mRNA in human tissues. All receptor mRNA levels were normalized to the level of GAPDH mRNA in the same tissue. A, GPR119 mRNA levels in commercially obtained samples of human total RNA from the indicated tissues. B, GPR119 mRNA expression in the indicated human tissues collected at autopsy (cerebrum) or at surgery (all tissues except cerebrum). C, Expression of GPR119, GPR40, GLP1R and SUR1 mRNA in normal human pancreatic tissue collected at surgery ($n=4$). The specimens used were the same as in panel B. Receptor mRNA levels in panels B and C are expressed as means ± SEM. *Black bar*, GPR119; *white bar*, GPR40; *hatched bar*, GLP1R; *double-hatched bar*, ABCC8 (SUR1).

Table 2 – The metabolic parameters and the levels of GPR119 mRNA in the pancreas of 19 patients.

Patient	BMI (kg/m^2)	FPG (mmol/L)	2 h-PG (mmol/L)	Insulin AUC ($\times 10^3$ pmol/L)	HbA1c (%)	HOMA-IR	Insulinogenic index	HOMA-beta	Triglycerides (mmol/L)	GPR119 mRNA level
1	24.2	4.7	6.7	32	5.1	9.6	83.0	124.4	1.23	0.183
2	19.7	7.2	12.6	53	7.1	36.6	100.1	102.1	2.26	0.334
3	17.7	4.4	6.8	24	5.1	2.8	62.7	50.8	1.54	0.430
4	22.3	4.9	9.1	18	5.7	3.7	17.8	40.3	0.89	0.112
5	24.6	5.1	8.3	25	5.1	5.7	42.8	54.0	1.20	0.235
6	25.7	6.1	*ND*	*ND*	5.6	24.0	*ND*	112.60	1.48	0.342
7*	22.1	2.0	4.9	84	4.7	2.5	*ND*	−61.3	0.86	0.419
8	18.0	5.3	10.8	12	6.3	3.3	23.6	25.1	1.76	0.063
9	19.6	4.3	11.4	*ND*	5.4	2.0	*ND*	40.8	2.01	0.228
10	20.0	4.6	6.9	24	5.0	8.4	163.7	130.7	1.40	0.583
11	22.8	5.5	13.6	*ND*	6.7	8.5	*ND*	58.0	2.28	0.483
12†	24.2	4.8	*ND*	*ND*	6.5	*ND*	*ND*	*ND*	1.01	0.582
13	23.3	5.2	10.7	18	5.8	8.5	11.1	70.8	1.29	0.185
14	24.3	*ND*	*ND*	*ND*	7.1	*ND*	*ND*	*ND*	0.95	0.272
15	23.5	4.9	8.9	*ND*	6.2	10.3	*ND*	113.8	1.99	0.492
16	18.4	6.1	*ND*	*ND*	6.5	*ND*	*ND*	*ND*	2.03	0.306
17†	16.8	5.1	*ND*	*ND*	5.8	*ND*	*ND*	*ND*	1.02	0.631
18	22.6	5.4	8.3	51	6.2	6.8	47.8	48.3	1.60	0.219
19	20.3	4.2	6.8	48	5.4	3.0	103.1	81.0	0.49	0.279

The patient numbers correspond to those in Table 1. *Patient 7 was diagnosed as having an insulinoma. †Patients 12 and 17 were treated with percutaneous transhepatic biliary drainage (PTBD). Because of the unavailability of blood samples, some of the metabolic profiles were not determined (shown as *ND*). *FPG*, fasting plasma glucose level; *2 h-PG*, 2-h post-OGTT plasma glucose level; *ND*, not determined.

Committee, Kyoto University Graduate School of Medicine, and were performed in accordance with institutional and national guidelines for animal experimentation. MIN6 cells were kindly provided by Dr. Junichi Miyazaki [34], and alpha-TC cells were obtained from American Type Culture Collection (ATCC) (Manassas, VA, USA). MIN6 cells were maintained in Dulbecco's modified Eagle's medium supplemented with 15% FBS, while alpha-TC cells were maintained in RPMI 1640 medium supplemented with 10% FBS. Both media also contained 100 U/mL penicillin and 0.1 mg/mL streptomycin (Life Technologies Japan, Tokyo, Japan). The cells were incubated at 37 °C under an atmosphere of humidified air (95%) and CO_2 (5%).

2.3. Total RNA preparation and cDNA synthesis

Total RNAs were extracted from fresh tissues and cell lines using QIAGEN RNeasy Mini Kits [9,10,33], and from FFPE tissue sections using QIAGEN RNeasy FFPE Kits (QIAGEN K.K., Tokyo, Japan). The collected RNA was then treated with DNase I to remove any contaminating DNA. Additionally, total RNAs from human brain, thyroid, heart, lung, trachea, kidney, esophagus, liver, skeletal muscle, adipose tissue, spleen, bladder, prostate, placenta and cervix were obtained from Life Technologies Japan. Total RNAs from stomach, small intestine, colon, pancreas, testis, ovary and uterus were from Takara Clontech (Tokyo, Japan). Finally, total RNAs from hypothalamus were obtained from two sources, Life Technologies Japan and BioChain Institute (Hayward, CA, USA). First strand cDNA was synthesized by random hexamer-primed reverse transcription using SuperScript II reverse transcriptase (Life Technologies Japan).

2.4. *Quantification of human and mouse receptor gene expression*

Levels of GPR119 mRNA in the pancreas and pancreatic islets were compared with those of GPR40, the glucagon-like peptide-1 receptor (GLP1R) and the sulfonylurea receptor 1 (ABCC8 or SUR1) mRNA, which are reportedly expressed in human pancreatic islets and involved in insulin secretion [9,10]. Messenger RNA levels were quantified using the TaqMan PCR method with an ABI PRISM 7700 Sequence Detector (Life Technologies Japan), as described previously [9,10]. To estimate the copy number of each mRNA, standard curves were generated using oligo DNA fragments (Sigma Genosys Japan, Tokyo, Japan) containing the PCR amplicon region. The receptor mRNA levels were normalized to the level of GAPDH mRNA and expressed as the receptor/GAPDH [copy/copy] ratio [9]. The sequences of the primers and probes (Life Technologies Japan) used for the quantification of the mRNAs were as follows: human *GPR119* (NM_178471), CCATGGCTGGAGGTTATCGA (forward), GCTCCCAATGAGAACA-GACACA (reverse) and 6-carboxyfluorescein (FAM)-CCCCACG-GACTCCCAGCGACT-6-carboxytetramethylrhodamine (TAMRA) (probe); mouse *GPR119* (NM_181751), TCCAGAGAGGACCAGA-GAAAGC (forward), GCAGCGTCTTAGCCATCGA (reverse) and FAM-TCACATCGTCACTATCAGCCATCCGG-TAMRA (probe); mouse *GPR40* (NM_194057), GGCTTTCCATTGAACTTGTTAGC (forward), CCCAGATGGAGAGTGTAGACCAA (reverse) and FAM-TGTCCCACGCTAAACTGCGACTCACTC-TAMRA (probe); mouse GADPH (NM_008084), TCCATGCCATCACTGCCA (forward), GCCCCACGGCCATCA (reverse) and FAM-CAGAAGACTGTG-GATGGCCCCTC-TAMRA (probe). The sequences of the primers and probes used for quantification of the human GPR40, GLP1R, ABCC8 (SUR1) and GAPDH mRNAs are described elsewhere [9,10].

2.5. *Data analysis on metabolic parameters*

We evaluated beta cell function and systemic insulin resistance using the insulinogenic index ($n=10$) [35] or the homeostasis model assessment of beta cell function (HOMA-beta) ($n=14$) and insulin resistance (HOMA-IR) ($n=14$) [36], respectively. The difference between the numbers of patients whose test data were included in the HOMA indices and insulinogenic index reflects the availability of data for plasma glucose and serum insulin levels at the 30 min mark during the oral glucose tolerance test (OGTT). The area under the serum insulin concentration–time curve (insulin AUC) was calculated from the OGTT data using the trapezoidal rule. Patients 7, 12 and 17 were excluded from analysis of the correlation between pancreatic GPR119 mRNA levels and metabolic parameters, because of a diagnosis of insulinoma (patient 7) or percutaneous transhepatic biliary drainage (patients 12 and 17). None of the patients were treated with oral glucose-lowering agents or with insulin. Table 2 shows the metabolic parameters of the patients whose pancreatic tissues were examined; the patient numbers correspond to those in Table 1.

2.6. *Statistical analysis*

Correlations between pancreatic GPR119 mRNA levels and clinical parameters were examined using the simple regression analysis. Differences between groups were assessed using unpaired two-tailed t tests or ANOVA where applicable. Values of $P<.05$ were considered significant (Statcel, Social Research Information, Tokyo, Japan).

3. Results

3.1. *Expression of GPR119 mRNA in normal human tissues*

We initially tested for GPR119 mRNA in samples of commercially available total RNA from normal human tissues. We found that the transcript was most abundant in the pancreas, followed by the gastrointestinal tract (small intestine, colon and stomach) and the testis (Fig. 1A). GPR119 mRNA was not detected in any other human tissue tested. To gain further insight into GPR119 gene expression humans and verify the aforementioned distribution profile, we also examined tissues obtained at surgery or autopsy. Among those samples, GPR119 mRNA was most abundant in the pancreas, followed by the duodenum, stomach, jejunum, ileum and colon, but was not detected in the esophagus, liver or cerebrum (Fig. 1B).

3.2. *Expression of GPR119, GPR40, GLP1R and SUR1 mRNAs in the human pancreas*

Using specimens from four patients, we compared the pancreatic expression of GPR119 mRNA with that of GPR40,

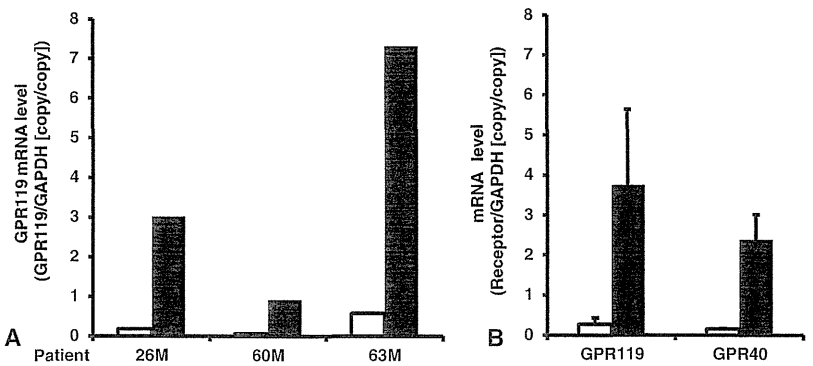

Fig. 2 – Expression of GPR119 mRNA in human pancreatic islets and adjacent pancreatic tissue. All receptor mRNA levels were normalized to the level of GAPDH mRNA in the same tissue. A, Comparison of GPR119 mRNA expression in pancreatic islets and adjacent pancreatic tissue from three patients. *White bars*, pancreas; *black bars*, pancreatic islets. B, Comparison of GPR119 and GPR40 mRNA expression in pancreatic islets and adjacent pancreatic tissue. The tissue samples used were the same as in panel A ($n=3$). Levels of GPR119 and GPR40 mRNA are expressed as means ± SEM. *White bars*, pancreas; *black bars*, pancreatic islets.

GLP1R and SUR1 mRNA in the same samples. We found that pancreatic levels of GPR119 mRNA were comparable to those of GPR40 mRNA and were higher than those of GLP1R and SUR1 mRNA (Fig. 1 C).

3.3. *Expression of GPR119 and GPR40 mRNA in isolated pancreatic islets and adjacent pancreatic tissue*

We next assessed GPR119 expression in pancreatic islets from three patients (Fig. 2A). Levels of GPR119 mRNA in freshly isolated islets were approximately 13 to 16 times higher than in the adjacent pancreatic tissue from the same patients. We also analyzed GPR40 expression and found that levels of GPR119 and GPR40 mRNA were similar in isolated pancreatic islets (Fig. 2B).

3.4. *Expression of GPR119 and GPR40 mRNA in human insulinomas and glucagonomas*

We also assessed expression of GPR119 and GPR40 mRNA using total RNAs extracted from specimens of fresh insulinomas ($n=2$), a glucagonoma ($n=1$) and a pancreatic acinar cell tumor ($n=1$), as well as from FFPE glucagonoma tissue sections from another patient ($n=1$). In the two cases of insulinoma, tumoral GPR119 mRNA levels were comparable to those in pancreatic islets (Fig. 3A). A considerable amount of GPR119 mRNA was also detected in tissue extracts from the glucagonoma (Fig. 3A), where GPR40 mRNA was not detectable (Fig. 3 C). Levels of GPR119 mRNA in tissue extracts from FFPE sections of non-tumor pancreas and glucagonoma were similar to those in the corresponding specimens collected at surgery (Fig. 3, A and B). GPR40 mRNA was not detected in extracts from the same FFPE glucagonoma sections (Fig. 3D), which is consistent with the level in the fresh tumor specimen (Fig. 3, C and D). Neither GPR119 nor GPR40 mRNAs was detectable in the acinar cell tumor specimen (Fig. 3, A and C).

3.5. *Expression of GPR119 and GPR40 mRNAs in mouse pancreatic islets, MIN6 insulinoma cells and alpha-TC glucagonoma cells*

To further explore GPR119 expression in pancreatic islet cells, we measured GPR119 mRNA levels in mouse pancreatic islets, MIN6 insulinoma cells and alpha-TC glucagonoma cells. We also assessed expression of GPR40 mRNA in the same samples, as GPR40 is known to be preferentially expressed in pancreatic beta cells in both rodents and humans [4,9,10,37]. High levels of GPR119 mRNA, comparable to those of GPR40 mRNA, were detected in mouse pancreatic islets (Fig. 4, A and B). Likewise, similar levels of GPR119 and GPR40 mRNA were detected in MIN6 cells (Fig. 4, A and B). On the other hand, the level of GPR119 mRNA in alpha-TC cells was approximately 1/7 that in MIN6 cells, and no GPR40 mRNA was detected in alpha-TC cells (Fig. 4, A and B).

3.6. *Correlation between pancreatic GPR119 mRNA expression and the insulinogenic index and HOMA-beta in humans*

To investigate the functional implications of pancreatic GPR119 expression in humans, we initially assessed GPR119 mRNA expression in non-tumor pancreatic tissue samples from 19 patients with various pancreatic tumors (Table 1). High levels of GPR119 mRNA, comparable to those in the four cases summarized in Fig. 1, A and B (0.336 ± 0.037 vs 0.319 ± 0.090), were detected in all of the tissue samples analyzed (Table 2). Because the inter-individual variation in the pancreatic GPR119 mRNA level ($n=19$) was high, to begin to explore the physiological importance of GPR119 in humans, we evaluated the relationship between pancreatic GPR119 mRNA levels and various clinical parameters. We found that GPR119 mRNA expression did not significantly differ among the head, body and tail portions of the pancreas (Table 3), nor did it correlate significantly with age (Supplemental Table S1).

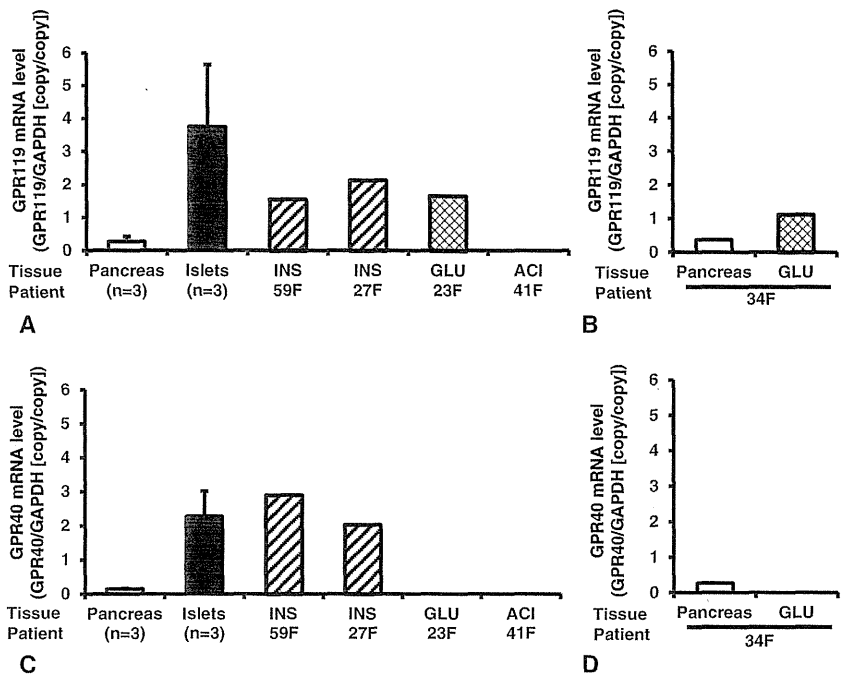

Fig. 3 – Expression of GPR119 and GPR40 mRNA in human pancreatic islets, insulinomas and glucagonomas. A and C, Expression of GPR119 (A) and GPR40 (C) mRNA in non-tumor pancreas (Pancreas), pancreatic islets (Islets), insulinomas (INS), a glucagonoma (GLU) and a pancreatic acinar cell tumor (ACI). B and D, Expression of GPR119 (B) and GPR40 (D) mRNA in extracts from non-tumor pancreatic and glucagonoma tissue sections ($n=1$ each). All receptor mRNA levels were normalized to the level of GAPDH mRNA in the same tissue. GPR119 and GPR40 mRNA levels in pancreas and pancreatic islets are expressed as means ±SEM. *White bars*, pancreas; *black bars*, pancreatic islets; *hatched bars*, insulinomas; *double-hatched bars*, glucagonomas.

When we then evaluated the correlation between pancreatic *GPR119* gene expression and several metabolic parameters, including glucose and triglyceride metabolism (Table 2), we found that pancreatic GPR119 mRNA levels did not correlate significantly with BMI, fasting plasma glucose (FPG), 2-h post-OGTT plasma glucose (2 h-PG), insulin AUC or fasting serum triglyceride levels (Supplemental Table S1), nor did they correlate significantly with HbA1c levels or HOMA-IR values (Supplemental Table S1, Fig. 5, A and B). By contrast, pancreatic GPR119 mRNA levels positively and significantly correlated with the insulinogenic index ($n=10$, $P=.004$, $r=0.817$) (Fig. 5 C) and with HOMA-beta values ($n=14$, $P=.043$, $r=0.547$) (Fig. 5D). Using the same patient data used to calculate the insulinogenic index ($n=10$) and HOMA-beta ($n=14$), we also tested for correlations

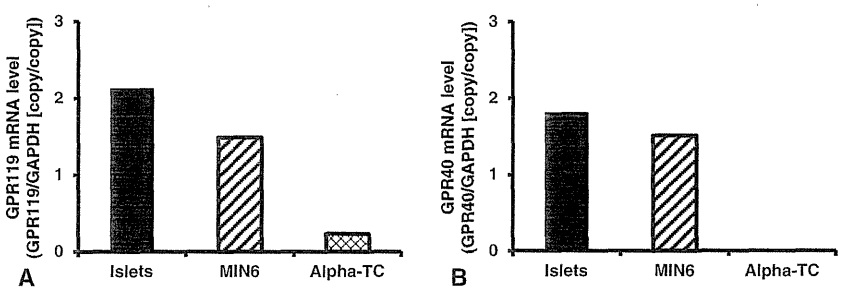

Fig. 4 – Expression of GPR119 and GPR40 mRNAs in mouse pancreatic islets, insulinoma and glucagonoma. Expression of GPR119 (A) and GPR40 (B) mRNAs pancreatic islets, MIN6 insulinoma cells and alpha-TC glucagonoma cells. All receptor mRNA levels were normalized to the level of GAPDH mRNA in the same tissue. *Black bars*, pancreatic islets; *hatched bars*, MIN6 cells; *double hatched bars*, alpha-TC cells.

Table 3 – GPR119 mRNA levels in various regions of the pancreas in humans.

Pancreatic region(s)	GPR119 mRNA level	n	P*
Head	0.372±0.052	11	-
Body	0.294±0.069	6	.388
Tail	0.262±0.079	2	.367
Body and tail	0.286±0.053	8	.264

GPR119 mRNA levels are expressed as means±SEM. Comparisons were made using unpaired two-tailed *t* tests.
* *P* values are vs the head.

between GPR119 mRNA expression and HbA1c levels and HOMA-IR values, which confirmed the absence of a significant correlation (Supplemental Table S1).

4. Discussion

Our findings demonstrate for the first time that GPR119 is highly expressed in human pancreatic islets, where the level of GPR119 expression is enriched more than 10-fold, as compared to adjacent areas of the pancreas in the same individuals. We also found that pancreatic levels of GPR119 mRNA are similar to those of GPR40 mRNA and are higher than those of GLP1R and SUR1 mRNA. Likewise, the level of GPR119 mRNA in isolated pancreatic islets is similar to that of GPR40 mRNA and higher than those of SUR1 and GLP1R mRNA [9,10]. This is noteworthy, as these receptors are reported to be abundantly expressed in human pancreatic islets.

We observed that substantial amounts of GPR119 mRNA are expressed in human insulinomas ($n=2$) and glucagonomas ($n=2$), and that the tumoral levels of the transcript are comparable to those in pancreatic islets. A similar pattern of GPR119 mRNA expression was also detected with mouse pancreatic islets, MIN6 insulinoma cells and alpha-TC glucagonoma cells. Thus GPR119 appears to be highly expressed in both beta and alpha cells in human and mouse pancreatic islets. Moreover, our observation that the expression levels of GPR119 and GPR40 mRNAs in human pancreatic islets are similar and are higher than that of SUR1 mRNA is noteworthy because SUR1 is reported to be abundantly expressed in both beta and alpha cells and is involved in the regulation of islet function, including insulin and glucagon secretion [38–40]. This strong expression suggests GPR119 may be involved in pancreatic islet function in humans. Consistent with that idea, pancreatic GPR119 mRNA levels correlated positively with two indices of beta cell function: the insulinogenic index and the HOMA-beta. Collectively, therefore, the present findings provide evidence for the possible involvement of GPR119 in islet function, perhaps affecting insulin secretion.

Using fresh tissue samples collected at surgery, we observed that, in humans, GPR119 mRNA is abundantly expressed in the small intestine, stomach and colon, but not in the esophagus. In rodents, GPR119 appears to be expressed in enteroendocrine cells, including L and K cells, and to be involved in the regulation of incretin and polypeptide YY secretion. In humans, enteroendocrine cells are distributed throughout the gastrointestinal tract, but not in the esophagus. Although details of GPR119 expression and its function in the human gastrointestinal tract will require further investigation, our findings are consistent with the idea that GPR119 is expressed in enteroendocrine cells and is involved in incretin and peptide YY secretion.

We detected no GPR119 mRNA in the human hypothalamus, brain or cerebrum, which is consistent with a recent report that GPR119 mRNA is not significantly expressed in the human brain or hypothalamus [19]. Although earlier reports using OEA (a putative GPR119 ligand) and a synthetic OEA analogue in rats suggest GPR119 may mediate signalling leading to reduced food intake and body weight, OEA appears

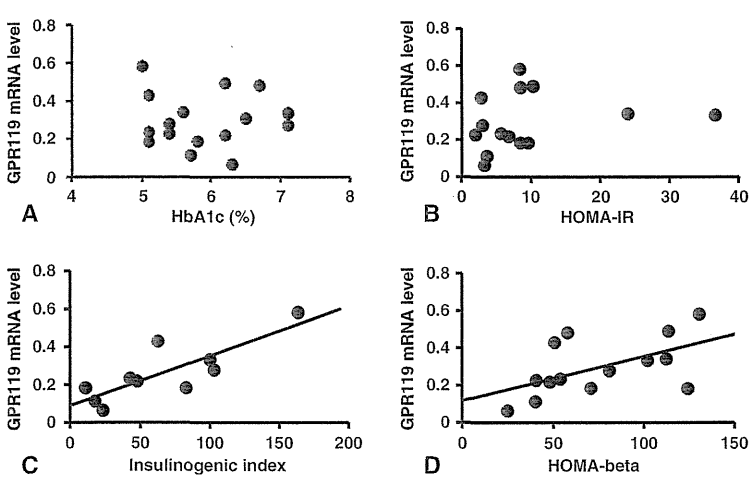

Fig. 5 – Correlations between human pancreatic GPR119 mRNA levels and parameters of glucose metabolism, including HbA1c levels ($n=16$) (A), HOMA-IR values ($n=14$) (B), the insulinogenic index ($n=10$) (C) and HOMA-beta values ($n=14$) (D). All GPR119 mRNA levels were normalized to the level of GAPDH mRNA in the same tissue. Simple regression analysis was used to determine *P* and *r* values. The solid lines are regression lines.

to act mainly in peripheral tissues, rather than in the central nervous system [41]. Our finding that GPR119 mRNA is highly expressed in the human stomach and duodenum is consistent with the notion that GPR119 is involved in regulating food intake in humans, as the bipolar vagal afferents involved in regulating feeding are known to project to the stomach and upper intestine [42,43].

In summary, the present study demonstrates that, in humans, GPR119 mRNA is abundantly expressed in healthy pancreatic islets and the human gastrointestinal tract, and in insulinomas and glucagonomas. The results provide evidence of an islet-gastrointestinal distribution of GPR119, its expression in pancreatic beta and alpha cells, and its possible involvement in islet function. They also provide the basis for a better understanding of the potential clinical importance of GPR119.

4.1. *Limitations of the present study*

Our study has several limitations that should be noted.

1. To our knowledge, no specific antibody against human GPR119 is available, so we were unable to assess expression of GPR119 protein.
2. The enrolled subjects were tumor-bearing patients, though the tumors were at an early stage or benign, and were resectable. Pancreatic biopsy is rarely performed because of the risk of pancreatitis, and is not justified in those without severe illness [44]. Therefore, we analyzed human pancreatic tissues collected during surgery. Because pancreatic tissue is very vulnerable to postmortem autolysis, specimens obtained at surgery offer substantial advantages for precise analysis of GPR119 expression. Nonetheless, possible weight loss and the paracrine effects of pancreatic cancer cells on beta cells could have influenced the correlation study.
3. Patients enrolled in the present study were not severely diabetic (HbA1c was less than 7.2%), nor were they overweight or obese (BMIs were less than 25). Thus clarification of the pathophysiological role of GPR119 in human diabetes and obesity must await further investigation in patients with a wider range of glucose tolerances and BMIs.
4. Plasma glucagon levels were not determined in the preoperative evaluation, and were not included in the present study. Beta cell mass is known to be much greater than alpha cell mass in pancreatic islets, and correlations between GPR119 mRNA levels and indices for beta cell function seem plausible, but may underestimate the involvement of GPR119 in the glucagon secretion. Further studies will be necessary to clarify the role of GPR119 in glucagon secretion.

Supplementary materials related to this article can be found online at http://dx.doi.org/10.1016/j.metabol.2012.06.010.

Author contributions

SO: data collection and analysis, data interpretation, manuscript writing. KH: data interpretation, manuscript writing. TT: data analysis, data interpretation, manuscript writing. JF, TK and KE: data interpretation, manuscript writing. YK, RD, KT, YS and SU: data collection, data interpretation. KN: data interpretation, manuscript writing.

Funding

This work was supported in part by the Ministry of Education, Culture, Sports, Science and Technology of Japan; Ministry of Health, Labor and Welfare of Japan; Takeda Medical Research Foundation; Smoking Research Foundation; Suzuken Memorial Foundation; Japan Foundation of Applied Enzymology; Novo Nordisk Insulin Research award; and Lilly Education and Research Grant Office. We gratefully acknowledge cooperative research program FINDS with Shionogi & Co., Ltd.

Acknowledgment

The authors acknowledge the technical assistance of Ms. A. Ryu of Kyoto University Graduate School of Medicine.

Conflict of interest

The authors have no conflict of interest to declare.

REFERENCES

[1] Stein DT, Stevenson BE, Chester MW, et al. The insulinotropic potency of fatty acids is influenced profoundly by their chain length and degree of saturation. J Clin Invest 1997;100:398–403.
[2] Lam TK, Pocai A, Gutierrez-Juarez R, et al. Hypothalamic sensing of circulating fatty acids is required for glucose homeostasis. Nat Med 2005;11:320–7.
[3] Fu J, Gaetani S, Oveisi F, et al. Oleylethanolamide regulates feeding and body weight through activation of the nuclear receptor PPAR-alpha. Nature 2003;425:90–3.
[4] Itoh Y, Kawamata Y, Harada M, et al. Free fatty acids regulate insulin secretion from pancreatic beta cells through GPR40. Nature 2003;422:173–6.
[5] Brown AJ, Goldsworthy SM, Barnes AA, et al. The orphan G protein-coupled receptors GPR41 and GPR43 are activated by propionate and other short chain carboxylic acids. J Biol Chem 2003;278:11312–9.
[6] Hirasawa A, Tsumaya K, Awaji T, et al. Free fatty acids regulate gut incretin glucagon-like peptide-1 secretion through GPR120. Nat Med 2005;11:90–4.
[7] Ahren B. Islet G protein-coupled receptors as potential targets for treatment of type 2 diabetes. Nat Rev Drug Discov 2009;8:369–85.
[8] Kebede MA, Alquier T, Latour MG, et al. Lipid receptors and islet function: therapeutic implications? Diabetes Obes Metab 2009;11(Suppl. 4):10–20.
[9] Tomita T, Masuzaki H, Iwakura H, et al. Expression of the gene for a membrane-bound fatty acid receptor in the pancreas and islet cell tumours in humans: evidence for GPR40 expression in pancreatic beta cells and implications for insulin secretion. Diabetologia 2006;49:962–8.

[10] Tomita T, Masuzaki H, Noguchi M, et al. GPR40 gene expression in human pancreas and insulinoma. Biochem Biophys Res Commun 2005;338:1788–90.
[11] Overton HA, Babbs AJ, Doel SM, et al. Deorphanization of a G protein-coupled receptor for oleoylethanolamide and its use in the discovery of small-molecule hypophagic agents. Cell Metab 2006;3:167–75.
[12] Lauffer LM, Iakoubov R, Brubaker PL. GPR119 is essential for oleoylethanolamide-induced glucagon-like peptide-1 secretion from the intestinal enteroendocrine L-cell. Diabetes 2009;58:1058–66.
[13] Hansen KB, Rosenkilde MM, Knop FK, et al. 2-Oleoyl glycerol is a GPR119 agonist and signals GLP-1 release in humans. J Clin Endocrinol Metab 2011;96:E1409–17, http://dx.doi.org/10.1210/jc.2011-0647.
[14] Chu ZL, Carroll C, Chen R, et al. N-oleoyldopamine enhances glucose homeostasis through the activation of GPR119. Mol Endocrinol 2010;24:161–70, http://dx.doi.org/10.1210/me.2009-0239.
[15] Soga T, Ohishi T, Matsui T, et al. Lysophosphatidylcholine enhances glucose-dependent insulin secretion via an orphan G-protein-coupled receptor. Biochem Biophys Res Commun 2005;326:744–51.
[16] Kogure R, Toyama K, Hiyamuta S, et al. 5-Hydroxy-eicosapentaenoic acid is an endogenous GPR119 agonist and enhances glucose-dependent insulin secretion. Biochem Biophys Res Commun 2011;416:58–63, http://dx.doi.org/10.1016/j.bbrc.2011.10.141.
[17] Ning Y, O'Neill K, Lan H, et al. Endogenous and synthetic agonists of GPR119 differ in signalling pathways and their effects on insulin secretion in MIN6c4 insulinoma cells. Br J Pharmacol 2008;155:1056–65.
[18] Chu ZL, Jones RM, He H, et al. A role for beta-cell-expressed G protein-coupled receptor 119 in glycemic control by enhancing glucose-dependent insulin release. Endocrinology 2007;148:2601–9.
[19] Chu ZL, Carroll C, Alfonso J, et al. A role for intestinal endocrine cell-expressed G protein-coupled receptor 119 in glycemic control by enhancing glucagon-like peptide-1 and glucose-dependent insulinotropic peptide release. Endocrinology 2008;149:2038–47.
[20] Lan H, Lin HV, Wang CF, et al. Agonists at GPR119 mediate secretion of GLP-1 from mouse enteroendocrine cells through glucose-independent pathways. Br J Pharmacol 2012;165:2799–807, http://dx.doi.org/10.1111/j.1476-5381.2011.01754.x.
[21] Semple G, Fioravanti B, Pereira G, et al. Discovery of the first potent and orally efficacious agonist of the orphan G-protein coupled receptor 119. J Med Chem 2008;51:5172–5.
[22] Lan H, Vassileva G, Corona A, et al. GPR119 is required for physiological regulation of glucagon-like peptide-1 secretion but not for metabolic homeostasis. J Endocrinol 2009;201:219–30.
[23] Gao J, Tian L, Weng G, et al. Stimulating beta-cell replication and improving islet graft function by AR231453, A gpr119 agonist. Transplant Proc 2011;43:3217–20, http://dx.doi.org/10.1016/j.transproceed.2011.10.021.
[24] Flock G, Holland D, Seino Y, et al. GPR119 regulates murine glucose homeostasis through incretin receptor-dependent and independent mechanisms. Endocrinology 2011;152:374–83.
[25] Semple G, Ren A, Fioravanti B, et al. Discovery of fused bicyclic agonists of the orphan G-protein coupled receptor GPR119 with in vivo activity in rodent models of glucose control. Bioorg Med Chem Lett 2011;21:3134–41, http://dx.doi.org/10.1016/j.bmcl.2011.03.007.
[26] Semple G, Lehmann J, Wong A, et al. Discovery of a second generation agonist of the orphan G-protein coupled receptor GPR119 with an improved profile. Bioorg Med Chem Lett 2011;22:1750–5, http://dx.doi.org/10.1016/j.bmcl.2011.12.092.
[27] Yoshida S, Ohishi T, Matsui T, et al. The role of small molecule GPR119 agonist, AS1535907, in glucose-stimulated insulin secretion and pancreatic beta-cell function. Diabetes Obes Metab 2011;13:34–41, http://dx.doi.org/10.1111/j.1463-1326.2010.01315.x.
[28] Cox HM, Tough IR, Woolston AM, et al. Peptide YY is critical for acylethanolamine receptor Gpr119-induced activation of gastrointestinal mucosal responses. Cell Metab 2010;11:532–42, http://dx.doi.org/10.1016/j.cmet.2010.04.014.
[29] Katz LB, Gambale JJ, Rothenberg PL, et al. Pharmacokinetics, pharmacodynamics, safety, and tolerability of JNJ-38431055, a novel GPR119 receptor agonist and potential antidiabetes agent, in healthy male subjects. Clin Pharmacol Ther 2011;90:685–92, http://dx.doi.org/10.1038/clpt.2011.169.
[30] Katz LB, Gambale JJ, Rothenberg PL, et al. Effects of JNJ-38431055, a novel GPR119 receptor agonist, in randomized, double-blind, placebo-controlled studies in subjects with type 2 diabetes. Diabetes Obes Metab 2012;14:709–16, http://dx.doi.org/10.1111/j.1463-1326.2012.01587.x; 10.1111/j.1463-1326.2012.01587.x.
[31] Vassilopoulos S, Esk C, Hoshino S, et al. A role for the CHC22 clathrin heavy-chain isoform in human glucose metabolism. Science 2009;324:1192–6.
[32] Seino Y, Nanjo K, Tajima N, et al. Report of the Committee on the Classification and diagnostic Criteria of Diabetes Mellitus. Diabetol Int 2010;1:2–20.
[33] Iwakura H, Hosoda K, Son C, et al. Analysis of rat insulin II promoter-ghrelin transgenic mice and rat glucagon promoter-ghrelin transgenic mice. J Biol Chem 2005;280:15247–56.
[34] Miyazaki J, Araki K, Yamato E, et al. Establishment of a pancreatic beta cell line that retains glucose-inducible insulin secretion: special reference to expression of glucose transporter isoforms. Endocrinology 1990;127:126–32.
[35] Ferrannini E, Gastaldelli A, Miyazaki Y, et al. beta-Cell function in subjects spanning the range from normal glucose tolerance to overt diabetes: a new analysis. J Clin Endocrinol Metab 2005;90:493–500.
[36] Matthews DR, Hosker JP, Rudenski AS, et al. Homeostasis model assessment: insulin resistance and beta-cell function from fasting plasma glucose and insulin concentrations in man. Diabetologia 1985;28:412–9.
[37] Briscoe CP, Tadayyon M, Andrews JL, et al. The orphan G protein-coupled receptor GPR40 is activated by medium and long chain fatty acids. J Biol Chem 2003;278:11303–11.
[38] Rajan AS, Aguilar-Bryan L, Nelson DA, et al. Sulfonylurea receptors and ATP-sensitive K+ channels in clonal pancreatic alpha cells. Evidence for two high affinity sulfonylurea receptors. J Biol Chem 1993;268:15221–8.
[39] Gribble FM, Reimann F. Sulphonylurea action revisited: the post-cloning era. Diabetologia 2003;46:875–91.
[40] Cooperberg BA, Cryer PE. Beta-cell-mediated signaling predominates over direct alpha-cell signaling in the regulation of glucagon secretion in humans. Diabetes Care 2009;32:2275–80.
[41] Rodriguez de Fonseca F, Navarro M, Gomez R, et al. An anorexic lipid mediator regulated by feeding. Nature 2001;414:209–12.
[42] Dockray GJ. The versatility of the vagus. Physiol Behav 2009;97:531–6.
[43] Engelstoft MS, Egerod KL, Holst B, et al. A gut feeling for obesity: 7TM sensors on enteroendocrine cells. Cell Metab 2008;8:447–9.
[44] Imagawa A, Hanafusa T, Uchigata Y, et al. Different contribution of class II HLA in fulminant and typical autoimmune type 1 diabetes mellitus. Diabetologia 2005;48:294–300.

nature medicine

Vitamin E decreases bone mass by stimulating osteoclast fusion

Koji Fujita[1,2], Makiko Iwasaki[1], Hiroki Ochi[3], Toru Fukuda[3], Chengshan Ma[1,2], Takeshi Miyamoto[4], Kimitaka Takitani[5], Takako Negishi-Koga[6], Satoko Sunamura[3], Tatsuhiko Kodama[7], Hiroshi Takayanagi[6], Hiroshi Tamai[5], Shigeaki Kato[8], Hiroyuki Arai[9], Kenichi Shinomiya[1], Hiroshi Itoh[3], Atsushi Okawa[1] & Shu Takeda[3]

Bone homeostasis is maintained by the balance between osteoblastic bone formation and osteoclastic bone resorption[1–3]. Osteoclasts are multinucleated cells that are formed by mononuclear preosteoclast fusion[1,2,4,5]. Fat-soluble vitamins such as vitamin D are pivotal in maintaining skeletal integrity. However, the role of vitamin E in bone remodeling is unknown. Here, we show that mice deficient in α-tocopherol transfer protein (*Ttpa*$^{-/-}$ mice), a mouse model of genetic vitamin E deficiency[6], have high bone mass as a result of a decrease in bone resorption. Cell-based assays indicated that α-tocopherol stimulated osteoclast fusion, independent of its antioxidant capacity, by inducing the expression of dendritic-cell–specific transmembrane protein, an essential molecule for osteoclast fusion, through activation of mitogen-activated protein kinase 14 (p38) and microphthalmia-associated transcription factor, as well as its direct recruitment to the *Tm7sf4* (a gene encoding DC-STAMP) promoter[7–9]. Indeed, the bone abnormality seen in *Ttpa*$^{-/-}$ mice was rescued by a *Tm7sf4* transgene. Moreover, wild-type mice or rats fed an α-tocopherol–supplemented diet, which contains a comparable amount of α-tocopherol to supplements consumed by many people, lost bone mass. These results show that serum vitamin E is a determinant of bone mass through its regulation of osteoclast fusion.

Bone mass is maintained constant from puberty until menopause by a balance between osteoblastic bone formation and osteoclastic bone resorption, a process called bone remodeling[1–3]. Osteoclasts are multinucleated polykaryons that develop from monocyte-lineage hematopoietic precursors through sequential steps: an initial phase of proliferation and a late phase of differentiation and maturation[1,2,10,11]. Hormones and cytokines have pivotal roles in osteoclast development. Specifically, macrophage colony-stimulating factor (M-CSF) and receptor activator of NF-κB ligand (RANKL) are indispensable for the proliferation of preosteoclasts and the differentiation and maturation of osteoclasts, respectively[1–3,12]. Among the fat-soluble vitamins A, D and K are well known for their ability to affect the skeleton[13,14], however, vitamin E was not examined well in the aspect of bone remodeling.

Vitamin E is a lipid-soluble antioxidant that inhibits lipid peroxidation by scavenging reactive oxygen species and is believed to be protective against arteriosclerotic change and the aging process[15]. Indeed, vitamin E is one of the most popular supplements in the United States; more than 10% of adults in the United States currently take vitamin E daily[16]. Vitamin E, which is a mixture of tocopherols and tocotrienols, is absorbed from food and is transported to the liver, where α-tocopherol transfer protein (α-TTP) mediates the selective transfer of α-tocopherol into lipoproteins[6]. Accordingly, α-tocopherol is the most predominant isoform of vitamin E in the body. Mice deficient in α-TTP (*Ttpa*$^{-/-}$ mice) show ataxia and infertility as a result of reduced serum α-tocopherol concentrations (**Fig. 1a**), which can be rescued by dietary supplementation with α-tocopherol[6,17].

To address the role of vitamin E in bone remodeling, we first studied *Ttpa*$^{-/-}$ mice. The *Ttpa*$^{-/-}$ mice developed a high-bone-mass phenotype in both their vertebrae and long bones as a result of a lower bone resorption compared to wild-type (WT) mice, as evidenced by a lowering of osteoclast surface and deoxypyridinoline, a bone resorption marker (**Fig. 1b–e** and **Supplementary Fig. 1**)[18]. In contrast, the amount of bone formation was unchanged in *Ttpa*$^{-/-}$ mice compared to WT mice. (**Fig. 1d**). This high-bone-mass phenotype was attributed to reduced serum concentrations of vitamin E (**Fig. 1a**) rather than the α-TTP deficiency in the body, as supplementation with α-tocopherol in the diet, which normalized the serum concentrations of α-tocopherol in *Ttpa*$^{-/-}$ mice (**Fig. 1f**), rescued the bone abnormality seen in *Ttpa*$^{-/-}$ mice (**Fig. 1g** and **Supplementary Fig. 2**). In line with this observation, *Ttpa*$^{+/-}$ mice, whose serum concentrations of α-tocopherol are between those of WT and *Ttpa*$^{-/-}$ mice[17], also had an

[1]Department of Orthopedic Surgery, Tokyo Medical and Dental University, Tokyo, Japan. [2]Global Center of Excellence (GCOE) Program, International Research Center for Molecular Science in Tooth and Bone Diseases, Tokyo Medical and Dental University, Tokyo, Japan. [3]Section of Nephrology, Endocrinology and Metabolism, Department of Internal Medicine, School of Medicine, Keio University, Tokyo, Japan. [4]Department of Orthopedic Surgery, School of Medicine, Keio University, Tokyo, Japan. [5]Department of Pediatrics, Osaka Medical College, Osaka, Japan. [6]Department of Cell Signaling, Graduate School of Medical and Dental Sciences, Tokyo Medical and Dental University, Tokyo, Japan. [7]Laboratory for Systems Biology and Medicine, University of Tokyo, Tokyo, Japan. [8]Institute of Molecular and Cellular Biosciences, University of Tokyo, Tokyo, Japan. [9]Department of Health Chemistry, Graduate School of Pharmaceutical Sciences, University of Tokyo, Tokyo, Japan. Correspondence should be addressed to S.T. (shu-tky@umin.ac.jp).

Received 14 July 2011; accepted 1 January 2012; published online 4 March 2012; corrected after print 4 May 2012; doi:10.1038/nm.2659

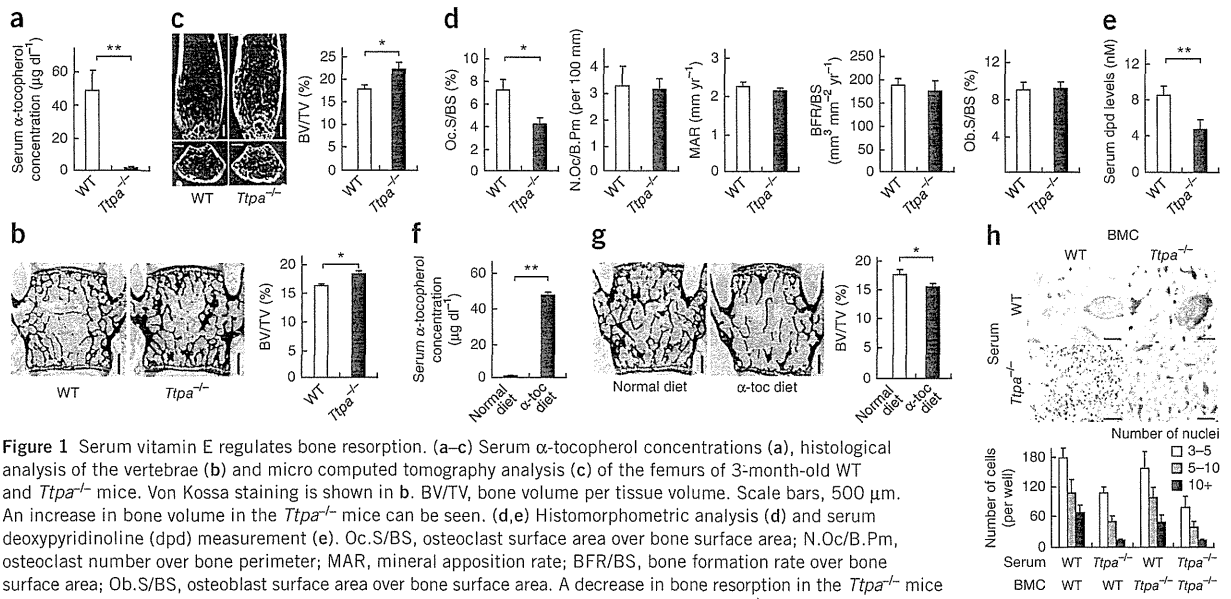

Figure 1 Serum vitamin E regulates bone resorption. (**a–c**) Serum α-tocopherol concentrations (**a**), histological analysis of the vertebrae (**b**) and micro computed tomography analysis (**c**) of the femurs of 3-month-old WT and *Ttpa*$^{-/-}$ mice. Von Kossa staining is shown in **b**. BV/TV, bone volume per tissue volume. Scale bars, 500 μm. An increase in bone volume in the *Ttpa*$^{-/-}$ mice can be seen. (**d**,**e**) Histomorphometric analysis (**d**) and serum deoxypyridinoline (dpd) measurement (**e**). Oc.S/BS, osteoclast surface area over bone surface area; N.Oc/B.Pm, osteoclast number over bone perimeter; MAR, mineral apposition rate; BFR/BS, bone formation rate over bone surface area; Ob.S/BS, osteoblast surface area over bone surface area. A decrease in bone resorption in the *Ttpa*$^{-/-}$ mice can be seen. (**f**,**g**) Serum α-tocopherol concentrations (**f**) and histological analysis (**g**) in *Ttpa*$^{-/-}$ mice fed a diet supplemented with α-tocopherol (α-toc diet). Von Kossa staining is shown in **g**. Scale bars, 500 μm. A decrease in bone volume as a result of the α-toc diet can be seen. (**h**) Serum α-tocopherol affects osteoclast differentiation. BMCs from the femurs of WT or *Ttpa*$^{-/-}$ mice were differentiated into osteoclasts in the presence of serum from WT or *Ttpa*$^{-/-}$ mice without addition of FBS. TRAP staining (left) and the number of osteoclasts (right) are shown. Scale bars, 50 μm. A decrease in the number of osteoclasts from WT BMCs with *Ttpa*$^{-/-}$ serum can be seen, whereas *Ttpa*$^{-/-}$ BMCs differentiated into osteoclasts normally with WT serum. $^{*}P < 0.05$, $^{**}P < 0.01$ by Tukey-Kramer testing (**b**) or Student's *t* test (**a**, **c–g**). All data are means ± s.e.m.

intermediate bone mass (**Supplementary Fig. 1b**). Moreover, osteoclast development *in vitro* was hampered when WT bone-marrow cells (BMCs) were cultured with the serum from *Ttpa*$^{-/-}$ mice (**Fig. 1h**), and this defect was ameliorated when this serum was supplemented with α-tocopherol or when serum from WT mice was used for the culture (**Fig. 1h** and **Supplementary Fig. 3**). In contrast, *Ttpa*$^{-/-}$ BMCs differentiated into osteoclasts normally when cultured with FBS or serum from WT mice (**Fig. 1h** and **Supplementary Fig. 3**). Thus, serum vitamin E regulates bone mass *in vivo* by affecting bone resorption.

Next, to examine the role of vitamin E in osteoclast development, we treated osteoclasts that were derived from WT BMCs and stimulated by RANKL with α-tocopherol *in vitro*. α-tocopherol stimulated osteoclast differentiation in a dose-dependent manner, as shown by an increase in the number of tartrate-resistant acid phosphatase (TRAP)-positive multinucleated osteoclasts (**Fig. 2a**), whereas the proliferation of osteoclast precursors and the survival of mature osteoclasts were unchanged by treatment with α-tocopherol (**Fig. 2b,c**). Osteoblastic differentiation and proliferation were not altered by α-tocopherol treatment (**Fig. 2d** and **Supplementary Fig. 4**), further indicating that vitamin E affects bone mass through osteoclasts rather than osteoblasts. Notably, α-tocopherol not only increased the generation of TRAP-positive multinucleated osteoclasts but also markedly increased the proportion of larger osteoclasts compared to the total osteoclasts (**Fig. 2e**), which indicated that vitamin E stimulated osteoclast maturation. As a result, α-tocopherol increased bone resorption by inducing the formation of additional mature osteoclasts (**Fig. 2f**).

Notably, α-tocopherol treatment administered only during the osteoclast maturation phase significantly increased osteoclast size and the number of nuclei per osteoclast (**Fig. 2e**), whereas α-tocopherol treatment administered at any other period did not have these effects (**Fig. 2e**), further indicating that vitamin E specifically affects late osteoclast maturation (that is, osteoclast fusion). Moreover, vitamin E also stimulated the generation of foreign-body giant cells, which are developed through macrophage fusion (**Fig. 2g**), further suggesting that vitamin E stimulates cell fusion. Indeed, the sizes of the TRAP-positive osteoclasts were smaller in the *Ttpa*$^{-/-}$ mice, which is in agreement with our *in vitro* observations (**Supplementary Fig. 2**). Taken together, the results suggest that vitamin E stimulates osteoclast fusion.

Because vitamin E is well known as an antioxidant[15], we next studied whether the antioxidant properties of vitamin E were indispensable for its ability to stimulate osteoclast fusion. With the exception of α-tocopherol, none of the isoforms of vitamin E, including α-tocotrienol, which is 100-fold stronger in antioxidant activity than α-tocopherol[15], stimulated osteoclast fusion (**Fig. 2h**). Moreover, except for α-tocopherol, none of the antioxidants tested, including ascorbic acid, which is the primary water-soluble antioxidant[19–22], stimulated osteoclast fusion (**Fig. 2i** and **Supplementary Fig. 5**). In line with these observations, hydrogen peroxide did not affect osteoclast fusion when it was present at a concentration that did not affect cell viability (**Supplementary Fig. 5**). Taken together, these results clearly show that, unlike other vitamin E isoforms and antioxidants, α-tocopherol specifically regulates osteoclast fusion independent of its antioxidant activity.

To address the molecular mechanism of the α-tocopherol–specific ability to stimulate osteoclast fusion, we analyzed the molecular markers of osteoclast differentiation after treatment with α-tocopherol. Among the many genes involved in osteoclast differentiation, only the expression of the differentiation marker genes, such as *Trap* and *Ctsk*[1,2,4,12], was increased, whereas the expression of other genes key for osteoclast differentiation, such as *Nfatc1* (nuclear factor of activated T cells c1)[1,2,4,12], was unchanged (**Fig. 3a**). We focused on

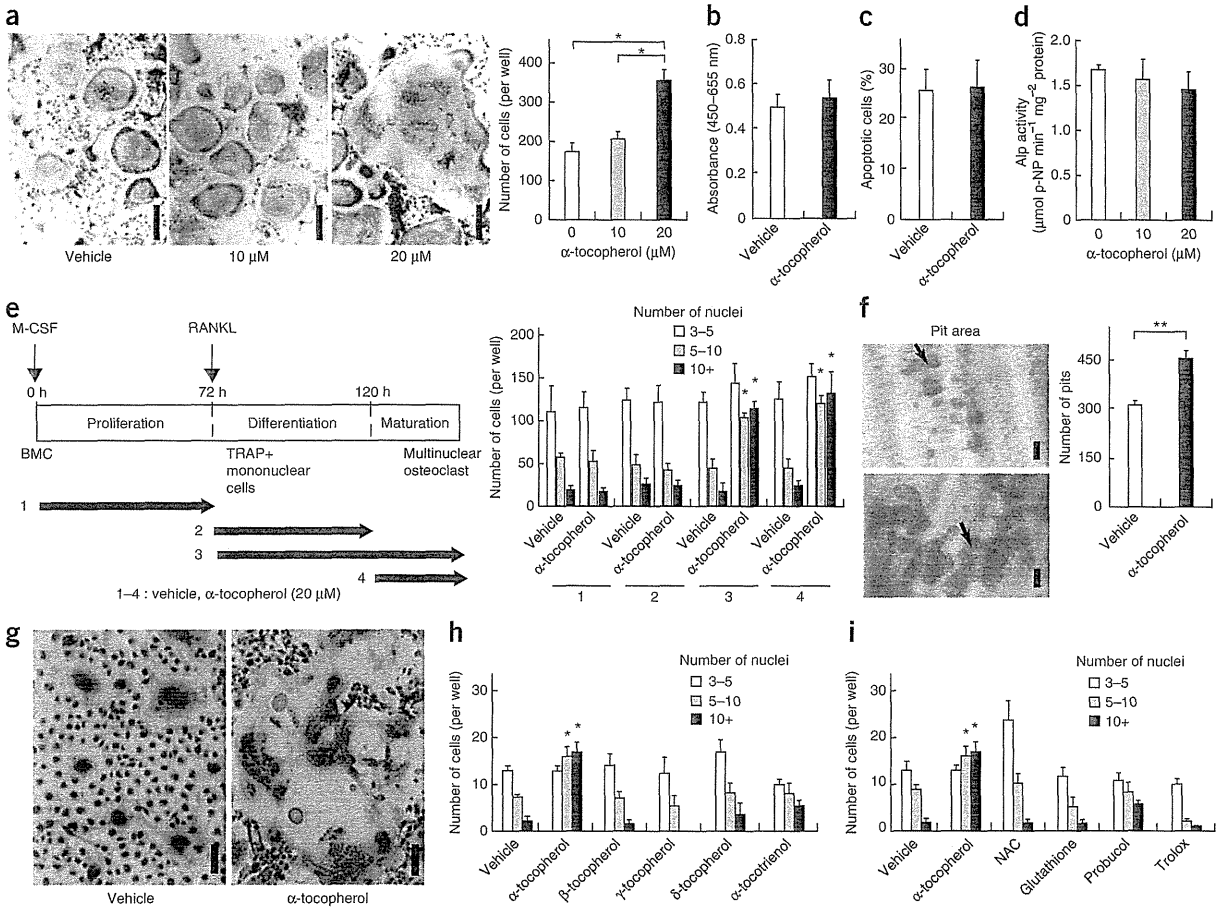

Figure 2 Vitamin E stimulates osteoclast fusion independent of its antioxidant activity. (**a–c**) The effect of α-tocopherol on osteoclast differentiation, proliferation and apoptosis. (**a**) BMCs were cultured with M-CSF, RANKL and 10% FBS. TRAP-stained cells (left) and the number of cells with more than three nuclei (right) are shown. An increase in osteoclasts after α-tocopherol treatment can be seen. (**b**) BrdU assay. BMCs were cultured with M-CSF, 10% FBS and α-tocopherol. (**c**) TUNEL assay. BMCs were cultured with M-CSF, RANKL and 10% FBS. (**d**) The effect of α-tocopherol on osteoblasts. An alkaline phosphatase (Alp) assay is shown. p-NP, p-nitrophenol. (**e**) The effect of α-tocopherol on osteoclast fusion. BMCs were cultured with M-CSF and RANKL, and α-tocopherol was added in the proliferation (1), differentiation (2 and 3) or maturation (3 and 4) phase. An increase in the proportion of multinucleated osteoclasts (3 and 4) can be seen. (**f**) The effect of α-tocopherol on bone resorption. A pit formation assay is shown. The eroded area (arrows, left) and the number of pits (right) are shown. BMCs were cultured on dentin with M-CSF and RANKL. α-tocopherol was added later. An increase in bone resorption can be seen. (**g**) Giant-cell progenitors from bone marrow were treated with α-tocopherol. (**h,i**) BMCs were cultured with M-CSF and RANKL. Vitamin E isoforms and antioxidants were added later. $^{*}P < 0.05$, $^{**}P < 0.01$ by Tukey-Kramer testing (**a**) or Student's *t* test (**f,h,i**). Scale bars, 50 μm. All data are means ± s.e.m.

dendritic-cell–specific transmembrane protein (DC-STAMP), a molecule essential for osteoclast fusion, because among the osteoclast-fusion–related genes[4,5], the gene encoding DC-STAMP (*Tmsf4*) was the only one whose expression was induced by α-tocopherol treatment (**Fig. 3a**). Notably, none of the other vitamin E isoforms induced *Tm7sf4* expression (**Fig. 3b**). Conversely, *Tm7sf4* expression was significantly decreased in *Ttpa*$^{-/-}$ mice, whereas expression of other fusion-related genes was unchanged, with the exception of osteoclast stimulatory transmembrane protein, which is another important molecule that is involved in osteoclast fusion (**Fig. 3c**)[23,24]. Next, to clarify the functional role of DC-STAMP in α-tocopherol–induced osteoclast fusion, we performed four sets of gain- and loss-of-function experiments for DC-STAMP. First, overexpression of *Tm7sf4* in RANKL-induced osteoclasts derived from WT mice markedly increased osteoclast fusion even in the absence of α-tocopherol (**Fig. 3d**). Conversely, although knockdown of *Nfatc1* in BMCs derived from WT mice eliminated the appearance of TRAP-positive mononuclear and multinuclear cells, knockdown of *Tm7sf4* only reduced the multinucleation of osteoclasts (that is, osteoclast fusion) (**Fig. 3e** and **Supplementary Fig. 6**), even in the presence of α-tocopherol. Moreover, osteoclast precursors isolated from *Tm7sf4*$^{-/-}$ mice did not differentiate into multinucleated osteoclasts in the presence of α-tocopherol (**Fig. 3f**). Furthermore, *Tm7sf4* transgenic mice[25] rescued the bone abnormality of the *Ttpa*$^{-/-}$ mice, as shown by a decreased bone volume accompanied by an increased bone resorption in the transgenic mice (**Fig. 3g** and **Supplementary Fig. 7**), which is consistent with the hypothesis that vitamin E induces osteoclast fusion through DC-STAMP. Taken together, these results indicate that the induction of DC-STAMP is necessary and sufficient for α-tocopherol to stimulate osteoclast fusion *in vitro* and *in vivo*.

Next, to gain insight into the molecular pathway of the induction of DC-STAMP by α-tocopherol, we examined whether α-tocopherol activates signaling pathways crucial for osteoclast differentiation. Among the pathways we studied, only the p38 pathway was specifically activated by α-tocopherol, as shown by the increase in phosphorylation of p38α, together with mitogen-activated protein kinase kinases 3 and 6 (Mkk3/6), a molecule that is upstream of p38α (**Fig. 4a** and **Supplementary Fig. 8**)[26]. Stimulation of p38α results in the downstream activation of the transcriptional regulator microphthalmia-associated transcription factor (Mitf)[27], an essential molecule for osteoclast maturation and fusion[1], and, indeed, treatment with α-tocopherol increased Mitf phosphorylation (**Fig. 4b**). Moreover, an antibody against Mitf immunoprecipitated the region containing the putative Mitf binding site in the *Tm7sf4* promoter (**Fig. 4c**), showing that Mitf binds to this site *in vivo*. To address the functional role of p38α and Mitf activation in α-tocopherol–induced osteoclast fusion, we knocked down *Tm7sf4* or *Mitf* in osteoclasts derived from WT mice. Knockdown of *Mapk14* (a gene encoding p38) or *Mitf* abolished the stimulatory effect of α-tocopherol on osteoclast fusion (**Fig. 4d**) and *Tm7sf4* induction (**Supplementary Fig. 6**). Conversely, overexpression of *Mapk14* significantly stimulated

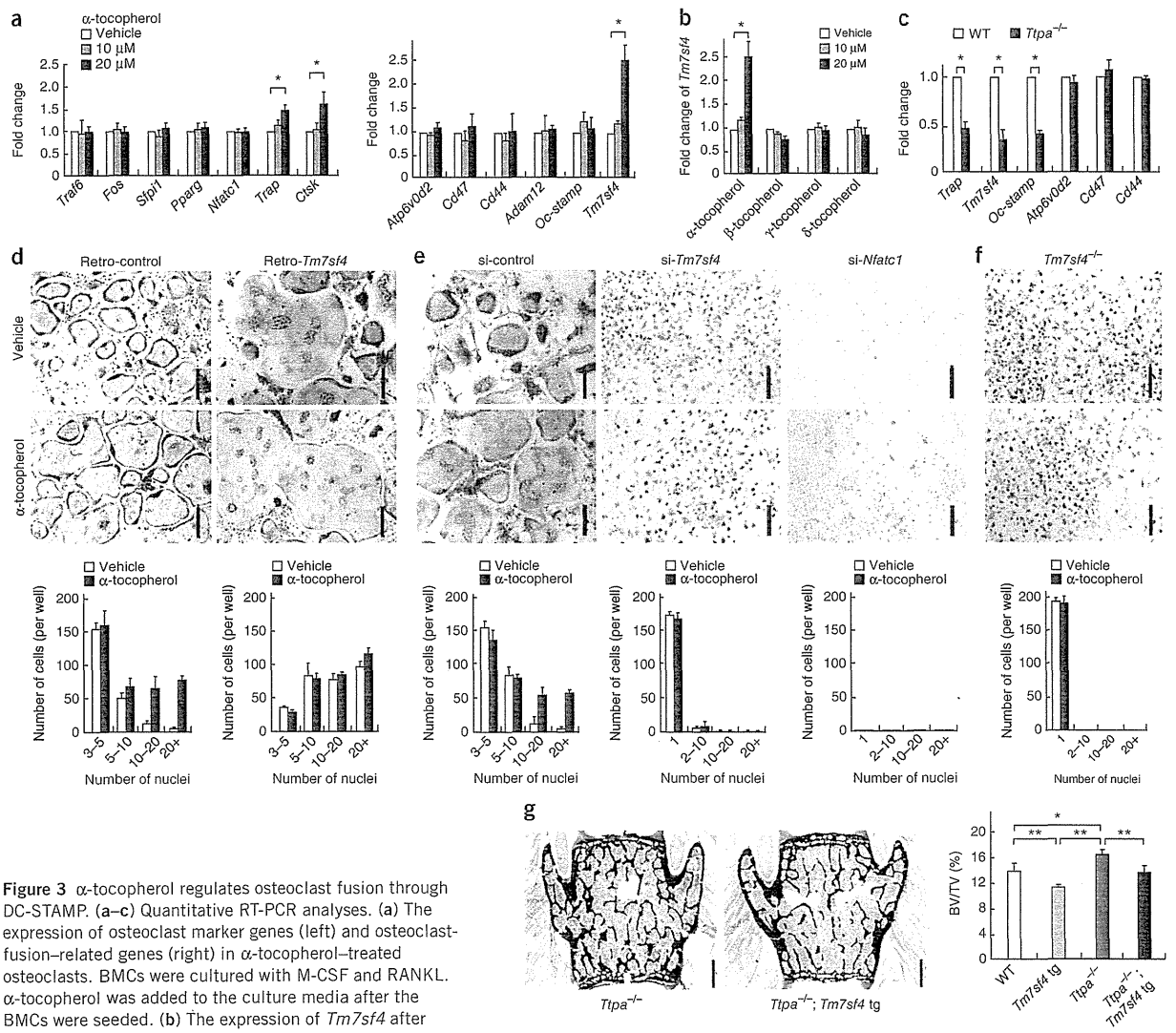

Figure 3 α-tocopherol regulates osteoclast fusion through DC-STAMP. (**a–c**) Quantitative RT-PCR analyses. (**a**) The expression of osteoclast marker genes (left) and osteoclast-fusion–related genes (right) in α-tocopherol–treated osteoclasts. BMCs were cultured with M-CSF and RANKL. α-tocopherol was added to the culture media after the BMCs were seeded. (**b**) The expression of *Tm7sf4* after treatment with various isoforms of vitamin E. (**c**) Expression of osteoclast-marker genes in WT and *Ttpa*$^{-/-}$ femurs. A decrease of the expression of *Tm7sf4* among the osteoclast-fusion–related genes can be seen. (**d–f**) DC-STAMP is essential for α-tocopherol–induced osteoclast fusion. (**d**) Retroviral overexpression of DC-STAMP. An increase in osteoclast fusion by DC-STAMP in the absence of α-tocopherol can be seen. Retro-*Tm7sf4*, retroviral overexpression of *Tm7sf4*; retro-control, retroviral overexpression of control vector. (**e,f**) The effect of α-tocopherol on siRNA-treated BMCs (**e**) and *Tm7sf4*$^{-/-}$ BMCs (**f**). si-control, non-targeting siRNA; si-*Tm7sf4*, siRNA to *Tm7sf4*; si-*Nfatc1*, siRNA to *Nfatc1*. A decrease in osteoclast fusion even in the presence of α-tocopherol can be seen. BMCs from WT (**d,e**) and *Tm7sf4*$^{-/-}$ (**f**) mice were cultured with M-CSF and RANKL. α-tocopherol was added to culture media after the BMCs were seeded. Scale bars, 50 μm. (**g**) Histological analysis of the vertebrae from WT, *Tm7sf4* transgenic (*Tm7sf4* tg), *Ttpa*$^{-/-}$ and *Ttpa*$^{-/-}$; *Tm7sf4* tg mice. Scale bars, 500 μm. $^{*}P < 0.05$, $^{**}P < 0.01$ by Tukey-Kramer testing (**a,b,g**) or Student's *t* test (**c**). All data are means ± s.e.m.

osteoclast fusion in the absence of α-tocopherol (**Fig. 4e**). These results clearly show that α-tocopherol regulates osteoclast fusion through p38α, Mitf and DC-STAMP. Currently, the molecular mechanism by which α-tocopherol induces p38α activation is unknown. A report showing that α-tocopherol succinate, which is a redox-silent analog of α-tocopherol, induces the activation of mitogen-activated protein kinase kinase kinase 5 (Ask-1)[28], which is an upstream protein kinase in the Mkk3/6-p38α pathway, suggests that α-tocopherol may use this same pathway in an antioxidant-independent manner.

Finally, to address the clinical relevance of our observations, we fed WT mice for 8 weeks with a diet containing an amount of α-tocopherol that is comparable to that found in supplements consumed by many people (**Fig. 4f**)[29]. WT mice fed a α-tocopherol–supplemented diet showed a 20% decreased bone mass after 8 weeks, with a concomitant increase in bone resorption and osteoclast size (**Fig. 4g,h** and **Supplementary Figs. 2** and **9**). Moreover, WT rats fed the same α-tocopherol–supplemented diet also had a 20% loss of bone mass after 8 weeks (**Fig. 4i** and **Supplementary Fig. 10**), showing that excessive intake of vitamin E is deleterious to maintaining bone mass in rodents. Notably, when WT mice were fed a diet supplemented with δ-tocopherol or antioxidants, we observed no bone loss (**Supplementary Fig. 9**), further indicating that α-tocopherol decreases bone mass independent of its antioxidant activity.

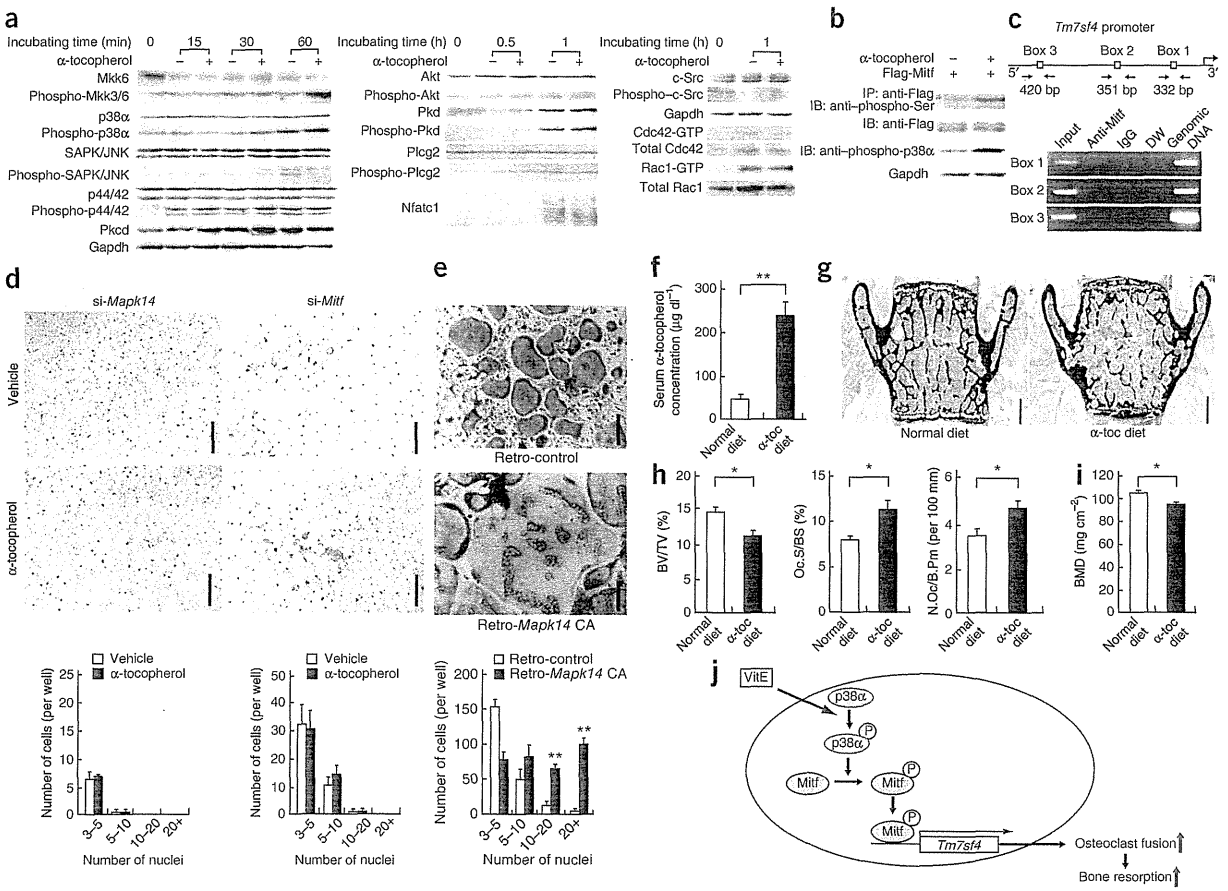

Figure 4 α-tocopherol decreases bone mass through p38α and Mitf. (**a**) Protein analysis of the α-tocopherol–treated osteoclasts. BMCs cultured with M-CSF only (left, middle) or mature osteoclasts that were induced by M-CSF and RANKL (right) were stimulated with α-tocopherol (20 μM) (– or +) and RANKL (middle right). Phospho-, phosphorylated; SAPK/JNK, mitogen-activated protein kinase 9 or mitogen-activated protein kinase 8; p44/42, mitogen-activated protein kinase 3 or cyclin-dependent kinase 20; Pkcd, protein kinase C, δ; Gapdh, glyceraldehyde-3-phosphate dehydrogenase; Akt, thymoma viral proto-oncogene 1; Pkd, protein kinase D; Plcg2, phospholipase C, γ 2; Nfatc1, nuclear factor of activated T cells, cytoplasmic, calcineurin dependent 1; c-Src, Rous sarcoma oncogene. (**b**) Immunoprecipitation analysis. An increase in the phosphorylation of p38α after treatment with α-tocopherol in p38α-expressing HEK293 cells can be seen. (**c**) Chromatin immunoprecipitation assay. Three potential binding sites (boxes 1–3) in the *Tm7sf4* promoter are shown (above). An antibody against Mitf (anti-Mitf) specifically immunoprecipitated the region containing the box 1 site of the *Tm7sf4* promoter. IgG, immunoglobulin G; DW, distilled water. (**d**,**e**) Gene knockdown (**d**) and retroviral overexpression (**e**) in osteoclasts. BMCs derived from WT mice were cultured with M-CSF and RANKL. α-tocopherol was added later. Scale bars, 50 μm. A decrease in osteoclast fusion even in the presence of α-tocopherol in BMCs treated with siRNA to *Mapk14* (si-*Mapk14*) (encoding p38α) or siRNA to *Mitf* (si-*Mitf*) (**d**) and an increase in osteoclast fusion in the absence of α-tocopherol in constitutively active p38α (*Mapk14*CA)-expressing BMCs (**e**) can be seen. (**f**–**h**) Analyses of WT mice and rats fed an α-tocopherol–supplemented diet. Serum α-tocopherol concentrations in these animals (**f**) and histological (**g**) and histomorphometric analyses (**h**). Scale bars, 500 μm. AA decrease in bone mass and an increase in bone resorption after α-tocopherol treatment can be seen. (**i**) Dual-energy X-ray absorptiometry analysis. A decrease in bone mineral density resulting from a α-tocopherol–supplemented diet. (**j**) The proposed mechanism of vitamin E (VitE)-induced osteoclastic fusion. P, phosphorylated. $^{*}P < 0.05$, $^{**}P < 0.01$ by Student's *t* test. All data are means ± s.e.m.

In summary, we show that vitamin E stimulates bone resorption and decreases bone mass by inducing osteoclast fusion (**Fig. 4j**). Moreover, we provide evidence that serum vitamin E is a determinant of bone mass. In contrast with our results, several reports have indicated that vitamin E participates in bone anabolism and that 6-hydroxy-2,5,7,8-tetramethylchroman-2-carboxylic acid (trolox), which is a vitamin E analog, inhibits inflammation-induced osteoclast differentiation[30–33]. In our experiments, trolox mildly inhibited osteoclast differentiation when we added it during the early osteoclast differentiation period (**Supplementary Fig. 11**), but it did not induce osteoclast fusion when we added it during the maturation phase (**Fig. 2i**). Alternatively, differences in the methodologies or the ages of the animals that were used in the previous compared to the present analyses may explain the discrepant results. In addition, several reports have shown the beneficial effects of α-tocopherol on human bone, which probably occur by reducing oxidative stress[21,34,35]. Nevertheless, most of these studies used a small sample size and were not well controlled. Given the widespread use of vitamin E, and especially α-tocopherol, as a supplement in humans, a larger, controlled study that addresses its effects on human bone is warranted.

METHODS

Methods and any associated references are available in the online version of the paper at http://www.nature.com/naturemedicine/.

Note: Supplementary information is available on the Nature Medicine website.

ACKNOWLEDGMENTS

We thank G. Karsenty, R. Baron and S. Tanaka for discussions; Y. Hotta, K. Miyamoto, H. Inose, S. Sato, A. Kimura, R. Xu and C. Xu for technical assistance; and T. Kitamura (Divisions of Cellular Therapy and Hematopoietic Factors, The Institute of Medical Science, The University of Tokyo, Tokyo, Japan) and I. Takada (Department of Microbiology and Immunology, Keio University School of Medicine, Tokyo, Japan) for plasmids. This work was supported by the Funding Program for Next Generation World-Leading Researchers (NEXT Program), grant-in-aid for scientific research from the Japan Society for the Promotion of Science, a grant for Global Center of Excellence Program from the Ministry of Education, Culture, Sports, Science and a Takeda Scientific Foundation grant.

AUTHOR CONTRIBUTIONS

K.F. conducted most of the experiments. M.I., H.O. and C.M. conducted mice analyses. T.F. and S.S. conducted *in vitro* experiments. T.M. provided DC-STAMP-related mice. K.T. and H. Tamai conducted the analyses of vitamin E serum concentrations. T.N.-K. performed western blots. H.A. provided *Ttpa*$^{-/-}$ mice. T.K. and H. Takayanagi conducted gene expression analyses. S.T., K.S., A.O. and H.I. designed the project. S.T. supervised the project and wrote most of the manuscript. S.K. designed the project.

COMPETING FINANCIAL INTERESTS

The authors declare no competing financial interests.

Published online at http://www.nature.com/naturemedicine/.
Reprints and permissions information is available online at http://www.nature.com/reprints/index.html.

1. Teitelbaum, S.L. & Ross, F.P. Genetic regulation of osteoclast development and function. *Nat. Rev. Genet.* **4**, 638–649 (2003).
2. Horne, W.C., Sanjay, A., Bruzzaniti, A. & Baron, R. The role(s) of Src kinase and Cbl proteins in the regulation of osteoclast differentiation and function. *Immunol. Rev.* **208**, 106–125 (2005).
3. Karsenty, G., Kronenberg, H.M. & Settembre, C. Genetic control of bone formation. *Annu. Rev. Cell Dev. Biol.* **25**, 629–648 (2009).
4. Lorenzo, J., Horowitz, M. & Choi, Y. Osteoimmunology: interactions of the bone and immune system. *Endocr. Rev.* **29**, 403–440 (2008).
5. Zou, W. & Teitelbaum, S.L. Integrins, growth factors, and the osteoclast cytoskeleton. *Ann. NY Acad. Sci.* **1192**, 27–31 (2010).
6. Yokota, T. *et al.* Delayed-onset ataxia in mice lacking α-tocopherol transfer protein: model for neuronal degeneration caused by chronic oxidative stress. *Proc. Natl. Acad. Sci. USA* **98**, 15185–15190 (2001).
7. Wagner, E.F. & Nebreda, A.R. Signal integration by JNK and p38 MAPK pathways in cancer development. *Nat. Rev. Cancer* **9**, 537–549 (2009).
8. Weilbaecher, K.N. *et al.* Linkage of M-CSF signaling to Mitf, TFE3, and the osteoclast defect in Mitf(mi/mi) mice. *Mol. Cell* **8**, 749–758 (2001).
9. Yagi, M. *et al.* DC-STAMP is essential for cell-cell fusion in osteoclasts and foreign body giant cells. *J. Exp. Med.* **202**, 345–351 (2005).
10. Vignery, A. Macrophage fusion: the making of osteoclasts and giant cells. *J. Exp. Med.* **202**, 337–340 (2005).
11. Bruzzaniti, A. & Baron, R. Molecular regulation of osteoclast activity. *Rev. Endocr. Metab. Disord.* **7**, 123–139 (2006).
12. Takayanagi, H. Osteoimmunology and the effects of the immune system on bone. *Nat. Rev. Rheumatol.* **5**, 667–676 (2009).
13. Kato, S. *et al.* The function of nuclear receptors in bone tissues. *J. Bone Miner. Metab.* **21**, 323–336 (2003).
14. Cockayne, S. *et al.* Vitamin K and the prevention of fractures: systematic review and meta-analysis of randomized controlled trials. *Arch. Intern. Med.* **166**, 1256–1261 (2006).
15. Azzi, A. *et al.* Specific cellular responses to α-tocopherol. *J. Nutr.* **130**, 1649–1652 (2000).
16. Radimer, K. *et al.* Dietary supplement use by US adults: data from the National Health and Nutrition Examination Survey, 1999–2000. *Am. J. Epidemiol.* **160**, 339–349 (2004).
17. Jishage, K. *et al.* α-tocopherol transfer protein is important for the normal development of placental labyrinthine trophoblasts in mice. *J. Biol. Chem.* **276**, 1669–1672 (2001).
18. Sato, S. *et al.* Central control of bone remodeling by neuromedin U. *Nat. Med.* **13**, 1234–1240 (2007).
19. Le Nihouannen, D., Barralet, J.E., Fong, J.E. & Komarova, S.V. Ascorbic acid accelerates osteoclast formation and death. *Bone* **46**, 1336–1343 (2010).
20. Ragab, A.A., Lavish, S.A., Banks, M.A., Goldberg, V.M. & Greenfield, E.M. Osteoclast differentiation requires ascorbic acid. *J. Bone Miner. Res.* **13**, 970–977 (1998).
21. Ruiz-Ramos, M., Vargas, L.A., Fortoul Van der Goes, T.I., Cervantes-Sandoval, A. & Mendoza-Nunez, V.M. Supplementation of ascorbic acid and α-tocopherol is useful to preventing bone loss linked to oxidative stress in elderly. *J. Nutr. Health Aging* **14**, 467–472 (2010).
22. Tsuneto, M., Yamazaki, H., Yoshino, M., Yamada, T. & Hayashi, S. Ascorbic acid promotes osteoclastogenesis from embryonic stem cells. *Biochem. Biophys. Res. Commun.* **335**, 1239–1246 (2005).
23. Yang, M. *et al.* Osteoclast stimulatory transmembrane protein (OC-STAMP), a novel protein induced by RANKL that promotes osteoclast differentiation. *J. Cell. Physiol.* **215**, 497–505 (2008).
24. Kim, M.H., Park, M., Baek, S.H., Kim, H.J. & Kim, S.H. Molecules and signaling pathways involved in the expression of OC-STAMP during osteoclastogenesis. *Amino Acids* **40**, 1447–1459 (2011).
25. Iwasaki, R. *et al.* Cell fusion in osteoclasts plays a critical role in controlling bone mass and osteoblastic activity. *Biochem. Biophys. Res. Commun.* **377**, 899–904 (2008).
26. Greenblatt, M.B. *et al.* The p38 MAPK pathway is essential for skeletogenesis and bone homeostasis in mice. *J. Clin. Invest.* **120**, 2457–2473 (2010).
27. Steingrimsson, E. *et al.* Mitf and Tfe3, two members of the Mitf-Tfe family of bHLH-Zip transcription factors, have important but functionally redundant roles in osteoclast development. *Proc. Natl. Acad. Sci. USA* **99**, 4477–4482 (2002).
28. Zu, K., Hawthorn, L. & Ip, C. Up-regulation of c-Jun–NH2-kinase pathway contributes to the induction of mitochondria-mediated apoptosis by α-tocopheryl succinate in human prostate cancer cells. *Mol. Cancer Ther.* **4**, 43–50 (2005).
29. Miller, E.R. III *et al.* Meta-analysis: high-dosage vitamin E supplementation may increase all-cause mortality. *Ann. Intern. Med.* **142**, 37–46 (2005).
30. Lee, J.H. *et al.* Trolox prevents osteoclastogenesis by suppressing RANKL expression and signaling. *J. Biol. Chem.* **284**, 13725–13734 (2009).
31. Arjmandi, B. *et al.* Vitamin E improves bone quality in the aged but not in young adult male mice. *J. Nutr. Biochem.* **13**, 543 (2002).
32. Mehat, M.Z., Shuid, A.N., Mohamed, N., Muhammad, N. & Soelaiman, I.N. Beneficial effects of vitamin E isomer supplementation on static and dynamic bone histomorphometry parameters in normal male rats. *J. Bone Miner. Metab.* **28**, 503–509 (2010).
33. Shuid, A.N., Mehat, Z., Mohamed, N., Muhammad, N. & Soelaiman, I.N. Vitamin E exhibits bone anabolic actions in normal male rats. *J. Bone Miner. Metab.* **28**, 149–156 (2010).
34. Chuin, A. *et al.* Effect of antioxidants combined to resistance training on BMD in elderly women: a pilot study. *Osteoporos. Int.* **20**, 1253–1258 (2009).
35. Ostman, B. *et al.* Oxidative stress and bone mineral density in elderly men: antioxidant activity of α-tocopherol. *Free Radic. Biol. Med.* **47**, 668–673 (2009).

ONLINE METHODS

Animals. We purchased the C57BL/6J mice from the Charles River Laboratory and Oriental Yeast, and we purchased the Wister rats from CLEA Japan. *Ttpa*$^{-/-}$, *Tm7sf4*$^{-/-}$ and *Tm7sf4* transgenic mice were previously described[6,9,25]. We crossed *Ttpa*$^{-/-}$ and *Tm7sf4* transgenic mice to obtain *Ttpa*$^{-/-}$; *Tm7sf4* transgenic mice. We fed the mice a diet supplemented with α-tocopherol (600 mg per kg of food; Sigma) from 4–12 weeks of age, and we fed the rats the same diet from 6–14 weeks of age. The α-tocopherol–supplemented diet was made by CLEA Japan. We analyzed seven or eight mice in each group. We maintained all animals under a 12-h light-dark cycle with *ad libitum* access to food and water. All animal experiments were performed with the approval of the Animal Study Committee of Tokyo Medical and Dental University and conformed to the relevant guidelines and laws.

Dual X-ray absorptiometry analyses. We measured the bone mineral density of the femurs of all animals by DCS-600 (ALOKA), as previously described[18]. We examined at least eight mice for each group.

Histological and histomorphometric analyses. We injected mice with calcein (25 mg per kg of body weight; Sigma) and stained the undecalcified sections of the lumbar vertebrae using von Kossa and TRAP, as previously described[18,36]. We performed static and dynamic histomorphometric analyses using the OsteoMeasure Analysis System (OsteoMetrics); the Oc.S/BS and N.Oc/B.pm values were calculated for the slices that stained positive for TRAP. We analyzed seven or eight mice in each group.

Cell culture. *In vitro* osteoclast differentiation was accomplished as previously described[18]. Briefly, BMCs of 6–8-week-old mouse femurs were cultured in minimum essential medium α supplemented with FBS in the presence of human M-CSF (10 ng ml^{-1}; R&D Systems) for 3 d and then differentiated into osteoclasts using human RANKL (50 ng ml^{-1}; PeproTech) and M-CSF for 3 d. The osteoclast culture using mouse serum is decribed in detail in the **Supplementary Methods**. The pit formation assay, BrdU assay and TUNEL assay were performed as previously described[18], and the details are described in the **Supplementary Methods**. The foreign-body giant-cell culture was established as previously described[37]. Briefly, BMCs were collected in DMEM (Sigma) with 10% FBS. Cells were stimulated with interleukin-4 (IL-4) (10 ng ml^{-1}) for 48 h, fixed and stained with May-Grünwald-Giemsa for evaluation. The *in vitro* primary osteoblast culture was established as previously described[38,39] (**Supplemntary Methods**). α-tocopherol was added to the culture media at 20 μM or at the indicated concentrations. Other vitamin E isoforms were added at 20 μM, N-acetylcysteine was added at 2 mM, glutathione was added at 5 mM, probucol was added at 5 μM and trolox was added at 200 μM. We cultured all cells in triplicate or quadruplicate wells and repeated each experiment more than three times. Additional details are given in the **Supplementary Methods**.

Transfection and retroviral infection. A total of 20 nM siRNA (Invitrogen) was transfected into BMCs derived from the femurs of WT mice using HiPerFect (QIAGEN). After transfection, cells were cultured using the same methods as those used for the osteoclast differentiation. Complementary DNA (cDNA) of *Tm7sf4* was cloned from osteoclasts using PCR. The constitutively active form of p38α was obtained from Addgene. Retrovirus was produced by the retroviral vector pMXs-IRES-GFP system, which was based on Moloney murine leukemia virus, as previously described[40]. Briefly, we collected the virus produced by packaging cells after 2 d of transfection. BMCs were infected with the retrovirus for 2 d in the presence of M-CSF. After 2 d of infection, cells were stimulated by RANKL to differentiate into osteoclasts. The details are described in the **Supplementary Methods**.

Quantitative RT-PCR analyses. To acquire RNA from mouse bones, we flushed bone marrow out of the femurs with PBS and used the bones as previously described[18]. RNA was extracted using TRIzol (Invitrogen), and reverse transcription was performed for cDNA synthesis using a High Capacity cDNA Reverse Transcription Kit (Applied Biosystems). We performed quantitative analyses of gene expression using the Mx3000P Real-Time PCR System (Stratagene). We examined the gene expressions in triplicate or quadruplicate individually and repeated each experiment more than three times.

Protein analyses. We collected cell lysate protein using radioimmunoprecipitation assay buffer with a phosphatase inhibitor cocktail (Nacalai) and the Complete Mini protease inhibitor cocktail (Roche). To detect RAS-related C3 botulinum substrate 1 (Rac1) and cell division cycle 42 (Cdc42) expression, we used Active GTPase Pull-Down and Detection kits (Thermo Scientific). For detecting the phosphorylation of Mitf, we used Anti-Flag M2 Affinity beads (Sigma), horseradish peroxidase–conjugated M2 antibody to Flag (1:1,000; Sigma) and antibody to phopshorylated serine (1:1,000; Millipore). Further details are given in the **Supplementary Methods**. We examined the expressions individually and repeated each experiment more than three times.

Chromatin immunoprecipitation (ChIP). We used ChIP-IT Express Chromatin Immunoprecipitation Kits (Active Motif), following the manufacturer's instructions. Briefly, we cultured BMCs from WT mice for 2 d. Cells were crosslinked with 0.4% formaldehyde, and the reaction was stopped by adding glycine. Fixed cells were resuspended in lysis buffer and sonicated for 5 min (with cycles of 30 s on and 30 s off). The supernatant was used immediately for ChIP experiments.

Statistical analyses. We performed statistical analyses using Tukey-Kramer testing for multiple comparisons and Student's *t* tests for two-group comparisons. Values were considered statistically significant at $P < 0.05$. All data are means ± s.e.m. Results are representative of more than four individual experiments.

Additional methods. Detailed methodology is described in the **Supplementary Methods**.

36. Kimura, A. *et al.* Runx1 and Runx2 cooperate during sternal morphogenesis. *Development* **137**, 1159–1167 (2010).
37. McNally, A.K., Macewan, S.R. & Anderson, J.M. Foreign body-type multinucleated giant cell formation requires protein kinase C β, δ, and ζ. *Exp. Mol. Pathol.* **84**, 37–45 (2008).
38. Ducy, P. *et al.* Leptin inhibits bone formation through a hypothalamic relay: a central control of bone mass. *Cell* **100**, 197–207 (2000).
39. Inose, H. *et al.* A microRNA regulatory mechanism of osteoblast differentiation. *Proc. Natl. Acad. Sci. USA* **106**, 20794–20799 (2009).
40. Kitamura, T. *et al.* Retrovirus-mediated gene transfer and expression cloning: powerful tools in functional genomics. *Exp. Hematol.* **31**, 1007–1014 (2003).